

DEVELOPMENT AND ANALYSIS OF AN ANIMAL MODEL OF  
AUTOSOMAL RECESSIVE HYPERCHOLESTEROLEMIA

APPROVED BY SUPERVISORY COMMITTEE

Helen H. Hobbs, M.D.

---

Joachim Herz , M.D.

---

Richard D. W. Anderson, Ph.D.

---

Phillip Shaul, M.D.

---

Joseph Albanesi, Ph.D.

---

---

## DEDICATION

To my parents

For their unwavering love and support.

DEVELOPMENT AND ANALYSIS OF AN ANIMAL MODEL OF  
AUTOSOMAL RECESSIVE HYPERCHOLESTEROLEMIA

by

CHRISTOPHER ERIC GRANGER JONES

DISSERTATION

Presented to the Faculty of the Graduate School of Biomedical Sciences

The University of Texas Southwestern Medical Center at Dallas

In Partial Fulfillment of the Requirements

For the Degree of

DOCTOR OF PHILOSOPHY

The University of Texas Southwestern Medical Center at Dallas

Dallas, Texas

April 2007



This work is licensed under the Creative Commons Attribution-Non  
Derivative Works 3.0 United States License. To view a copy of this  
license, visit <http://creativecommons.org/licenses/by-nd/3.0/us/> or send a  
letter to Creative Commons, 543 Howard Street, 5th Floor, San Francisco,  
California, 94105, USA.

by

Christopher Eric Granger Jones, 2007

Some Rights Reserved

MOUSE MODEL OF AUTOSOMAL RECESSIVE  
HYPERCHOLESTEROLEMIA

Publication No. \_\_\_\_\_

Christopher Eric Granger Jones

The University of Texas Southwestern Medical Center at Dallas, 2007

Supervising Professors: Joachim Herz, M.D. & Helen Hobbs, M.D.

The low density lipoprotein receptor (LDLR) in the liver is the major route of removal of LDL cholesterol (LDL-C) from the blood. Defects in *LDLR* cause familial hypercholesterolemia (FH), which is characterized by elevated LDL-C, premature coronary atherosclerosis, and autosomal dominant inheritance. A similar clinical picture with an autosomal recessive mode of inheritance occurs in autosomal recessive hypercholesterolemia (ARH). ARH is caused by mutations in the *ARH*

gene, which encodes for a putative adaptor protein implicated in linking the LDLR to the endocytic machinery. To determine the role of ARH in LDLR function, mice that do not express ARH were developed via targeted gene disruption. Similarly to ARH patients, *Arh*<sup>-/-</sup> mice have fractional catabolic rates (FCRs) for LDL similar *Ldlr*<sup>-/-</sup> mice, yet have much less severe elevations in LDL-C when fed normal chow. Upon cholesterol feeding, however, plasma lipoprotein profiles between *Ldlr*<sup>-/-</sup> and *Arh*<sup>-/-</sup> were indistinguishable. Immunolocalization studies reveal normal sorting but defective internalization of LDLRs in the livers of *Arh*<sup>-/-</sup> mice. Whereas the clearance of LDL was markedly and similarly delayed in the *Arh*<sup>-/-</sup> and *Ldlr*<sup>-/-</sup> mice, the rate of removal of VLDL was significantly higher in *Arh*<sup>-/-</sup> mice compared to *Ldlr*<sup>-/-</sup> animals. Primary hepatocytes expressing human LDLRs rapidly accumulated fluorescently labeled  $\beta$ -VLDL, but failed to internalize labeled LDL, monoclonal anti-LDLR antibody, or antibody:Protein A tetramers in the absence of ARH. These findings indicate ARH is caused by delayed clearance of LDL by LDLRs in the liver, but the severity of the disease is ameliorated by preserved VLDL clearance in the absence ARH. Thus the lower levels of LDL-C in ARH compared to FH are due to reduced production of LDL from VLDL.

## TABLE OF CONTENTS

LIST OF FIGURES .....	ix
LIST OF TABLES.....	x
LIST OF ABBREVIATIONS .....	xii
I. INTRODUCTION .....	1
II. METHODS .....	15
III. CHARACATERIZATION OF ARH-DEFICIENT MICE .....	31
IV. ARH SUBDOMAINS .....	45
V. XANTHOMATOSIS .....	54
VI. VLDL METABOLISM IN ARH .....	59
VII. CONCLUSIONS .....	79
BIBLIOGRAPHY .....	93

## PRIOR PUBLICATIONS

Jones C, Garuti R, Michaely P, Li WP, Maeda N, Cohen JC, Herz J, Hobbs HH. Disruption of LDL but not VLDL clearance in autosomal recessive hypercholesterolemia. (2007) *J Clin Invest*. **117**, 165-74.

Garuti, R, Jones, C, Li, W-P, Michaely, P, Herz, J, Gerard, RD, Cohen, JC, Hobbs HH. The modular adaptor protein ARH promotes LDLR clustering into clathrin-coated pits. (2005) *J Biol Chem* **280**, 40996-1004.

Jones C, Hammer RE, Li WP, Cohen JC, Hobbs HH, Herz J. Normal sorting but defective endocytosis of the low density lipoprotein receptor in mice with autosomal recessive hypercholesterolemia. (2003) *J Biol Chem* **278**, 29024-30.

Weeber EJ, Beffert U, Jones C, Christian JM, Forster E, Sweatt JD, Herz J. Reelin and ApoE receptors cooperate to enhance hippocampal synaptic plasticity and learning. (2002) *J Biol Chem* **277**, 39944-52.

Goodrich LD, Lin TC, Spicer EK, Jones C, Konigsberg WH. Residues at the carboxy terminus of T4 DNA polymerase are important determinants for interaction with the polymerase accessory proteins. (1997) *Biochemistry* **36**, 10474-81.

Abdus Sattar AK, Lin TC, Jones C, Konigsberg WH. Functional consequences and exonuclease kinetic parameters of point mutations in bacteriophage T4 DNA polymerase. (1996) *Biochemistry* **35**, 16621-9.

## LIST OF FIGURES

FIGURE 1-1 .....	13
FIGURE 1-2 .....	14
FIGURE 3-1 .....	40
FIGURE 3-2 .....	41
FIGURE 3-3 .....	42
FIGURE 3-4 .....	43
FIGURE 3-5 .....	44
FIGURE 4-1 .....	50
FIGURE 4-2 .....	51
FIGURE 4-3 .....	52
FIGURE 5-1 .....	58
FIGURE 5-2 .....	59
FIGURE 6-1 .....	68
FIGURE 6-2 .....	69
FIGURE 6-3 .....	70
FIGURE 6-4 .....	71
FIGURE 6-5 .....	72
FIGURE 6-6 .....	73
FIGURE 6-7 .....	74

FIGURE 6-8 .....	75
FIGURE 6-9 .....	77

## LIST OF TABLES

TABLE 3-1 .....	39
TABLE 6-1 .....	67



## LIST OF DEFINITIONS

$\alpha$ 2M – alpha 2-macroglobulin

ARH – autosomal recessive hypercholesterolemia

$\beta$ -VLDL – beta-migrating very low density lipoprotein

Dil – 1,1'-dioctadecyl-3,3,3',3'-tetramethylindocarbocyanine perchlorate

FCR – fractional catabolic rate

FH – familial hypercholesterolemia

FPLC – fast performance liquid chromatography

HDL – high density lipoprotein

HSPG – heparin sulfate proteoglycan

LDL – low density lipoprotein

LDL-C – low density lipoprotein cholesterol

LDLR – low density lipoprotein receptor

LRP – low density lipoprotein receptor related protein

PAGE – polyacrylamide gel electrophoresis

PBS – phosphate buffered saline

PMCA-O – 3-pyrenemethyl-23, 24-dinor-5-cholen-22-oate-3 beta-yl oleate

PTB – phosphotyrosine binding

## **CHAPTER ONE**

### **INTRODUCTION**

In 1973 Khachadurian and Uthman described a Lebanese family in which the four offspring all had elevated plasma cholesterol levels (mean 728 mg/dl) and large tendinous xanthomas [1]. While the clinical presentation of these four siblings resembled homozygous familial hypercholesterolemia (FH), the disease appeared to be genetically distinct. Neither parent had significantly elevated plasma cholesterol levels, indicating a recessive mode of inheritance. Over the next several decades, characterization of similar patients with severe hypercholesterolemia and recessive inheritance [2, 3] led to the identification of a new monogenic form of hypercholesterolemia. This new disorder was termed autosomal recessive hypercholesterolemia (ARH). ARH was initially described as a phenocopy of homozygous FH, yet as more ARH patients were examined subtle yet distinct differences between the two disorders have emerged.

#### **Familial hypercholesterolemia**

FH is characterized by an elevated concentration of LDL and cholesterol deposition in tissues in the form of xanthomas and atheroma,

leading to premature arteriosclerosis and coronary heart disease. FH is an inherited autosomal dominant disorder and one of the most common inborn errors of metabolism, with a gene frequency of 1:500 in most populations [4]. FH is caused by mutations in the *LDLR* gene and is inherited in an autosomal dominant pattern. The low-density lipoprotein receptor (LDLR) is a central coordinator of the metabolism of cholesterol. Loss of LDLR function due to mutations leads to defective clearance of LDL from the blood and an accumulation of plasma cholesterol. Patients who are homozygous for mutations in the *LDLR* gene (FH homozygotes) have essentially no functioning LDLRs and a much more severe phenotype than their heterozygous counterparts. FH homozygotes have plasma cholesterol levels ranging from 600 mg/dl to 1200 mg/dl. In these patients clinically significant coronary artery disease is often apparent within first decade of life, and planar and tendinous xanthomas (depositions of cholesterol) develop almost uniformly by age 4 [4]. FH homozygotes respond only modestly to current drug therapies, such as the HMG-CoA reductase inhibitors (statins) and ezetimibe, a drug that interferes with cholesterol absorption, even when given at high doses [5]. In spite of multi-drug therapy, LDL cholesterol (LDL-C) levels typically remain elevated, and these patients require routine LDL aphaeresis.

### **Clinical Features of ARH**

Examination of patients with ARH from Sardinia [6] and Japan [7] revealed severe elevations in plasma cholesterol levels, ranging from 400 mg/dl to 650 mg/dl. In almost all patients examined plasma levels of triglycerides and HDL cholesterol were normal. Metabolic characterization of ARH patients revealed fractional catabolic rates (FCR) of LDL as low as those of FH homozygotes [2, 8]. In spite of comparable LDL FCRs in FH and ARH patients, characterization of additional ARH patients from unrelated families has revealed less severe mean plasma cholesterol elevations in patients with ARH [4, 6, 9-12].

Another characteristic of ARH patients is the presence, often from childhood, of large, bulky xanthomas. The extent of xanthoma formation is typically proportional to the duration and severity of the elevation in plasma LDL [4]. ARH patients, however, often present with profound xanthomatosis in excess of their plasma cholesterol levels when compared to FH homozygotes [1, 3, 7]. The lesions do regress and can disappear if cholesterol levels can be adequately reduced by drug therapy [13]. Only three ARH patients described thus far lack xanthomas, though two of them began lipid-lowering therapies before age 8 [14]. The pathophysiology of xanthoma formation in ARH has not been investigated, but has been hypothesized to be related to preserved LDLR activity in

perivenular macrophage, which may accelerate accumulation of cholesterol and foam cell formation [6]. One study, however, has found monocyte-derived macrophage from two ARH patients to be defective at internalization and degradation of LDL, suggesting the mechanism of xanthoma formation may be more complex [9].

Patients with ARH appear to respond to cholesterol-reducing drug therapy much more effectively than FH homozygotes. Arca, *et al.* observed 30%-60% reductions in LDL-C in 21 ARH patients during their treatment with statins [6]. Others have reported normalization of plasma cholesterol levels on combined drug therapy alone [13]. These results are a stark contrast to resistance the patients lacking LDLRs have shown to the unbecoming effects of high-dose drug therapy [15, 16]. Moderate success (up to 30% reduction in LDL-C) has been reported with high dose simvastatin and atorvastatin in FH homozygotes with residual LDLR activity [17, 18], but the response was not nearly as great as that seen in patients with ARH. Thus ARH was originally described as a phenocopy of homozygous FH, the published data suggest that in addition to having lower levels of LDL-C, ARH patients on average have a later onset of coronary artery disease, more severe xanthomatosis, and a superior response to lipid-lowering drug therapy than homozygous FH patients. The basis for the for the less severe hypercholesterolemia in ARH and the

better response of patients to drug therapy is not clear and requires further investigation into the mechanism of the disease.

### **Role of the ARH in LDLR Function**

Using pedigrees from Sardinian and Lebanese families, Garcia *et al.* mapped the defect in ARH to a gene on chromosome 1p36-35 [10]. The gene, dubbed *ARH*, codes for a modular adaptor protein containing a single phosphotyrosine binding (PTB) domain and is expressed in all tissues, with the highest mRNA levels in liver and kidney [10]. Mutations in *ARH* have been reported in all patients with ARH. The mutations characterized to date introduce premature stop codons, as a result of point mutations, frameshifts, or inappropriate splicing [9, 10, 19-22]. ARH protein has not been detected in any cell extracts from patients by immunoblotting, despite the presence of normal amounts of mRNA in some mutant cell lines [9, 10, 22]; essentially all ARH patients as yet described are null for the ARH protein.

Much of the original work that led to an understanding of the role of the LDLR in cellular cholesterol homeostasis was performed by analyzing the binding, uptake, and degradation of <sup>125</sup>I-labeled LDL in skin fibroblasts cultured from patient biopsies. Fibroblasts from FH patients expressing no LDLRs fail to bind, internalize, or degrade LDL efficiently [23]. In contrast,

fibroblasts derived from ARH patients are able to internalize and degrade  $^{125}\text{I}$ -labelled LDL at normal rates, initially excluding defective LDLR function the cause of ARH [2, 7].

Biodistribution studies, however, suggested a cell-type specific role for ARH. Zuliani *et al.* injected  $^{99\text{m}}\text{Tc}$ -labeled LDL into ARH patients and compared the uptake in several organs with normolipidemic controls and an FH homozygote [2]. Hepatic LDL uptake was as defective in the ARH probands as the FH homozygote. Uptake of LDL was also reduced in the spleen and kidney of the two patients.

At the same time, the first direct evidence of a biochemical defect in LDLR function was revealed from characterization of Epstein-Barr virus (EBV) transformed lymphocytes from two unrelated pairs of siblings with ARH. EBV immortalized lymphocytes derived from FH patients have previously been used similarly to fibroblast as a cell culture model to analyze LDLR function [24]. Lymphocytes from ARH patients demonstrated defective LDLR-dependent LDL internalization despite normal expression of LDLR mRNA and protein [25]. ARH lymphocytes were able to bind LDL normally, but the all the LDLR accumulated on the cell surface, supporting a role for ARH in LDLR internalization. EBV-transformed lymphocytes are currently the only experimental model in which to investigate ARH function.

### **ARH and clathrin coated pit endocytosis**

The *ARH* gene is found in vertebrates, including zebrafish. Alignment of the protein sequences from several species reveals five highly conserved domains (Fig. 1-1). The N-terminal portion of the protein consists of a conserved 30 amino acid domain not found in any other protein and of unknown function. The PTB domain follows from amino acids 30-174. A pentapeptide type I clathrin binding consensus sequence encoded by residues 212-216 is similar to motifs found in several clathrin coated pit accessory proteins [26]. In the C-terminus are two conserved regions. First, a sequence that binds the  $\beta_2$ -adaptin subunit of AP-2, and then the last four amino acids, which are predicted to bind a type II PDZ domain.

The most striking feature of ARH is the PTB domain. PTB domains are found in many adaptor proteins known to bind NPXY motifs in the cytoplasmic domains of cell surface receptors, including other LDL receptor family members [27-29]. The PTB domain of ARH displays significant identity to the PTB domains of Disabled-1 (Dab1, 29%) and Disabled-2 (Dab2, 22%), both of which have been implicated in the protein trafficking and signaling of LDLR family members [29-31]. The PTB domain of Dab1 binds to the NPXY motif on the cytoplasmic tails of the

VLDL receptor and apolipoprotein E (apoE) receptor-2 and plays a central role in cortical lamination in the developing brain by transducing Reelin signaling [32]. Dab2 has been implicated in regulating the trafficking and endocytosis of megalin, another LDLR family member, in the proximal tubule of the kidney. Mice lacking Dab2 excrete the megalin ligands vitamin A and vitamin D binding proteins into their urine, consistent with a deficiency in megalin endocytosis [30]. This defect, however, is not as severe as in mice devoid of megalin itself [33], suggesting that some megalin activity is preserved.

The cytoplasmic tail of the LDLR contains a single NPXY motif that is required for clustering and endocytosis of the receptors in fibroblasts [27, 34]. Point mutations in this highly conserved sequence have been found in patients with FH [34, 35]. Of particular interest is the well-characterized FH patient J.D., who is a compound heterozygote for the LDLR with one null allele and a point mutation leading to expression cysteine for the tyrosine in the NPXY motif (Y807C) on the second [34]. Cultured skin fibroblasts from J.D. expressing LDLRs with the Y807C mutation bound LDL normally but failed to internalize the receptor [36]. Disruption of other residues either immediately before or in the NPXY itself was later shown to disrupt internalization of the receptor as well without

altering LDL binding, demonstrating the requirement of the sequence FDNPVY for LDLR internalization [27].

This immediately suggested a role for ARH in LDLR endocytosis. Pull down experiments confirmed the PTB domain of ARH can interact with the canonical internalization sequence of the LDLR, FDNPVY, and mutation of this sequence eliminates binding *in vitro* [37, 38]. Other LDLR family members contain NPXY consensus sequences in their cytoplasmic tails, but were not examined. It is not known whether ARH binds these sequences or plays a physiological role in the activity of these receptors.

The LDLR-related protein (LRP), in particular, contains two NPXY motifs, yet it is not known whether either can interact with ARH. Similar in function to the LDLR, LRP participates in the removal from the circulation by the liver of apoE containing lipoproteins, such as IDL and chylomicron remnants [39]. In the initial ARH patients examined, an accumulation of chylomicron remnants was not reported [2]. Nevertheless, a partial defect in LRP activity may not have been detected under the experimental conditions under which the patients were examined and could contribute to the hyperlipoproteinemia observed in ARH.

Another group has reported a functional relationship between ARH and megalin endocytosis in transfection models [31]. Megalin has three NPXY motifs, one of which binds Dab2 and is required for efficient

endocytosis [29]. Whether ARH plays a physiological role in megalin function has yet to be determined. As yet ARH patients have not been reported to have any other disorders unrelated to LDLR function, but the widespread expression of ARH suggests it may play other roles.

Recombinant ARH also binds with high affinity to phosphatidylinositol 4,5-bisphosphate (PtdIns(4,5)P<sub>2</sub>), the terminal domain of the clathrin heavy chain and the  $\beta_2$ -adaptin subunit of AP-2 via conserved domains in its C-terminus [37, 38]. The capacity of ARH to bind clathrin suggests that ARH may couple NPXY-containing receptors to the clathrin-mediated endocytosis machinery. Interestingly, AP-2 also synchronously binds clathrin and PtdIns(4,5)P<sub>2</sub>. The association of AP-2 with clathrin is through a canonical type I clathrin binding sequence (LLNLD) in the  $\beta_2$ -subunit of AP-2 [40].

Other clathrin coated pit adaptor proteins show similar redundancy in binding with their partners. The G-protein coupled receptor (GPCR) adaptor proteins, the  $\beta$ -arrestins, modulate GPCR activity by directing the internalization of activated receptors. The  $\beta$ -arrestins also bind PtdIns(4,5)P<sub>2</sub>, AP-2, and clathrin [41-43]. Internalization of activated GPCRs is dependent upon the capacity of the  $\beta$ -arrestins to bind these components of the clathrin-mediated endocytosis machinery. Although ARH associates with identical components of the endocytic machinery as

the  $\beta$ -arrestins, the relative contribution of each of these interactions and the role of seemingly redundant interactions is unknown due to the absence of naturally occurring point mutations within these domains of ARH. ARH is hypothesized to link the LDLR to the clathrin-mediated endocytosis machinery and oversee LDLR internalization during the early events of endocytosis (Fig. 1-2).

### **Areas of investigation**

While the ARH phenotype primarily results from apparent LDLR deficiency in the liver, studies in humans have only been able to investigate directly the role of ARH in peripheral tissues, such as fibroblasts and lymphocytes. Due to the inability to directly study the cell biological features of hepatocytes from affected humans, I have created a mouse model of ARH to examine the role of ARH in LDLR activity and the function LDLR family members in the liver and other tissues. Through complementation assays I have also investigated the contribution of ARH interactions with various components of clathrin coated pit machinery. These animals provide an experimental model to study the effects of ARH deficiency on cholesterol homeostasis in the intact organism and investigate the basis for the subtle differences in phenotype between ARH and homozygous FH.

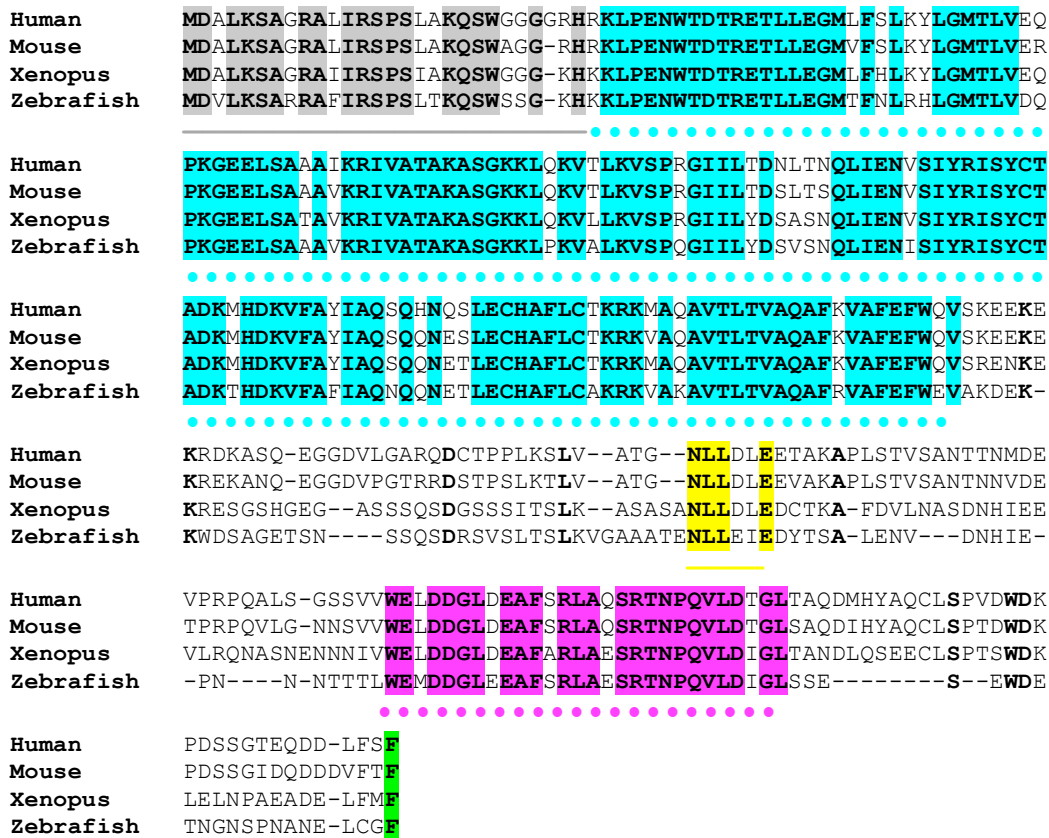


**Fig. 1-1** – Alignment of ARH protein sequences from human, mouse, *Xenopus laevis*, and zebrafish. Conserved residues across all four species are in bold. Grey – conserved N-terminal domain; blue – PTB domain; yellow – clathrin box consensus sequence; violet –  $\beta_2$ -adaplin binding site; green – putative type II PDZ domain binding site.

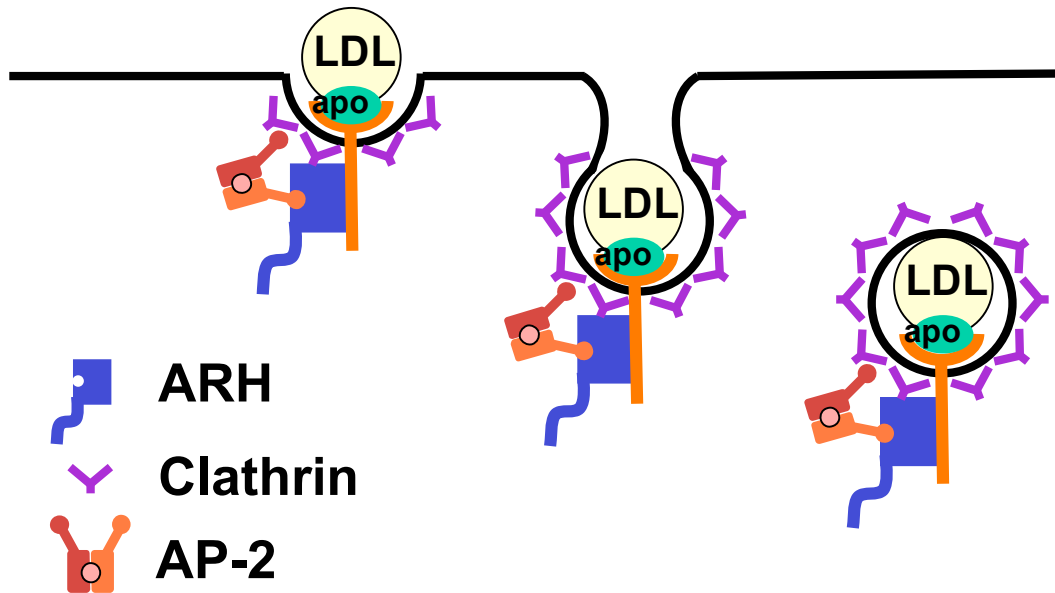


**Fig 1-2** – Model for multiple interactions of ARH with clathrin coated pit machinery. ARH binds clathrin, AP-2 and guides the LDLR through the early events of endocytosis. The C-terminus of ARH contains a putative type II PDZ domain binding sequence. The physiological role of this sequence is unknown.

## CHAPTER TWO

### METHODS

#### General Methods –

Unless otherwise indicated, DNA manipulations were performed using standard techniques [44]. Cholesterol and triglycerides were determined enzymatically with assay kits obtained from Roche Biochemicals (Indianapolis, IN) and Sigma Chemicals, (St. Louis, MO), respectively [45]. Plasma lipoprotein fraction were separated by fast performance liquid chromatography (FPLC) using a Superose 6 column (Amersham Biosciences, Piscataway, NJ) and cholesterol concentrations were determined as described [46, 47]. Protein concentrations were determined using the method of Lowry [48]. Methylamine-activated  $\alpha$ 2-macroglobulin was the generous gift of Dr. Dudley Strickland (University of Maryland School of Medicine, Rockville, MD). Asialofetuin was generated by incubating 100 mg fetuin (Sigma) at 37°C in 10 ml 100 mM sodium acetate, pH 5.0, 2 mM CaCl<sub>2</sub> together with 1 unit of neuraminidase-type XA (Sigma) immobilized on agarose beads. After 4 h another unit of neuraminidase was added, and the incubation was continued overnight. Both  $\alpha$ 2M and asialofetuin were radiolabeled with <sup>125</sup>I using the iodogen method [49].

**Antibodies –**

Rabbit polyclonal antibodies against Rab5 (KAP-GP006), EEA1 (324610), and GRP78 (BiP) (SPA-826) were purchased from StressGen Biotechnologies (Victoria, BC, Canada) and Calbiochem (San Diego, CA), respectively. Rabbit polyclonal antibodies against Lamp1 (H-228) and Rab11 (H-87) were purchased from Santa Cruz Biotechnology (Santa Cruz, CA). The polyclonal antibody against mouse ARH was raised in rabbits using the PTB domain of mouse ARH fused to glutathione S-transferase. A rabbit polyclonal antibodies against the LDLR and human ARH were raised using the C-terminal 13 residues of mouse LDLR and ARH, respectively, fused to keyhole limpet hemocyanin. Rabbit polyclonal antibodies against LRP and purified LDLR from bovine adrenal have been described elsewhere [50, 51]. The anti-LDLR monoclonal antibody, IgG-C7, and the monoclonal antibody against an irrelevant antigen, IgG-2001, have been described elsewhere [52, 53].

**Animals and diets –**

All mice used experimentally were maintained on a hybrid genetic background of C57Bl6/J and 129Sv strains. Mice with a genetic disruption of *Ldlr* were previously described [54]. Mice expressing the human LDLR

at the endogenous mouse *Ldlr* locus (*hLDLR* knock-in mice) [55] were a generous gift from Dr. Nobuyo Maeda (University of North Carolina, Chapel Hill, NC). All mice were housed on a 12-hour dark/12-hour light cycle and maintained on standard chow containing 6% (w/w) animal fat and 0.02% (w/w) cholesterol (Teklad 6% mouse/rat diet 7002, Harlan-Teklad, Madison, WI) and water *ad libitum* unless otherwise stated. The Western diet was synthesized by supplementing normal chow with 21% (w/w) anhydrous milk fat and 0.2% (w/w) cholesterol. The Paigen diet contained normal chow supplemented with 21% (w/w) anhydrous milk fat, 1.25% (w/w) cholesterol, 0.5% (w/w) cholic acid. The high-carbohydrate diet (no. 960237, MP Biomedicals, Aurora, OH) contained 60.2% sucrose, 20% casein, 15% cellulose, 0.3% DL-methionine, 3.5% minerals and vitamins, and <0.2% fat. All animal experiments were approved by the University of Texas Southwestern Medical Center Animal Care and Use Committee (IACUC) and were performed according to all applicable federal animal welfare policies and regulations.

### **Lipoproteins –**

Mouse LDL ( $d$  1.025-1.50 g/ml) was isolated by sequential ultracentrifugation [56] from pooled plasma obtained from *Ldlr*<sup>-/-</sup> mice [54] that had been fasted >6 h. Mouse VLDL ( $d$ <1.006) was isolated by

ultracentrifugation from pooled plasma obtained after an overnight fast from *Ldlr*<sup>-/-</sup> mice fed a Paigen diet for 2 weeks, as described [57]. Mouse lipoproteins were radiolabeled with <sup>125</sup>I by the iodine monochloride method as described [56]. Human LDL (*d* 1.019-1.063 g/ml) was prepared by sequential ultracentrifugation from the plasma of healthy human volunteers after a 12-hour fast [56].  $\beta$ -VLDL (*d* <1.006) was isolated from the plasma of cholesterol fed rabbits as described [58]. Human LDL and rabbit  $\beta$ -VLDL were radiolabeled using the Bolton-Hunter reagent [59] purchased from Amersham Biosciences (Piscataway, NJ). Fluorescent LDL (PMCA-O LDL) was synthesized by reconstituting the LDL core with 3-pyrenemethyl-23, 24-dinor-5-cholen-22-oate-3 beta-yl oleate (PMCA-O) as described [60] with minor modifications. After reconstitution with PMCA-O, fluorescently labeled LDL monomers were separated from aggregated LDL via FPLC using a Superose 6 column.  $\beta$ -VLDL was fluorescently labeled with 1,1'-dioctadecyl-3,3,3',3'-tetramethylindocarbocyanine perchlorate (DiI) as described [61]. Colloidal gold-labeled LDL (LDL-gold) and colloidal gold-labeled  $\beta$ -VLDL (VLDL-gold) were produced using methods previously described for the production of LDL-gold [62]. Briefly, 100 ml of 10% (w/v) gold chloride was added to 100 ml of boiling water. After 10 sec, 2 ml of 1% trisodium citrate was added and the mixture was maintained at 100°C for 5 min. The reaction

was cooled to 25°C, adjusted to a pH of 6.0 with dipotassium phosphate and then centrifuged at 800 x g for 30 min at 4°C to remove aggregates. The colloidal gold was collected by centrifugation at 17,500 x g for 40 min at 4°C. The centrifuged material was aspirated to a volume of 1 ml. The colloidal gold pellet was resuspended and added to an equal volume of human LDL or  $\beta$ -VLDL (1 mg/ml), which had been dialyzed overnight against 50 mM EDTA, pH 6.0. After allowing the mixture to incubate at room temperature (60 min), the mixture was overlaid on a 35% sucrose cushion and spun at 17,500 x g for 60 min at 12°C. The gold conjugate in the pellet was resuspended in PBS (2.5 ml), solvent exchanged over a PD-10 column (Pharmacia-Amersham) equilibrated in PBS and dialyzed twice against 3 L of PBS at 4°C. Labeled lipoproteins were used within 5 days of synthesis.

#### **Cloning of mouse ARH cDNA –**

Murine ARH cDNA was amplified from a commercially available mouse liver cDNA library (Clontech, Palo Alto, CA) using the following primers: 5'-ATTCTAGACATGGACGCGCTCAAGTCGGCG-3' and 5'-TTAAGCTTTCAGAAGGTGAAGACGTCATCATC-3'. Amplification products were TA cloned into pCR2.1-TOPO (Invitrogen, Carlsbad, CA) and sequenced.

### Generation of ARH knockout mice –

Two fragments were amplified from genomic DNA from mouse liver (129S6/SvEv strain) using long-range PCR (Takara Biochemical, Inc., Berkeley, CA). An 8.5 kb fragment, corresponding to a region extending from intron 4 into the 3'-untranslated region, was derived using primers 5LA1 5'-ACG**GCGGCCG**CCTGTGTGGCCTGAGTCCCTCCCTGG-3' and 3LA1 5'-CCT**GCGGCCG**CCGCCAGCATGAGCAAGC-3', and a 1 kb fragment containing part of intron 3 was amplified using primers 5SA 5'-ACG**CTCGAG**GTGTGCCAGTGGGGAACCAGGAAGG-3' and 3SA 5'-TGC**CTCGAG**GGGAGATGGAAATAAGAAATGAAGGAAGC-3'. The two fragments were cloned into the targeting vector [63] on either side of a PGK*neobpA* expression cassette [64] using *Not I* and *Xho I* sites, respectively. The vector also contained two copies of the herpes simplex virus thymidine kinase gene [65] in tandem at the 5' end of the short arm. The linearized vector was electroporated into murine embryonic stem cells SM1 and recombinant clones were selected using G418 and gangcyclovir, as described [66]. Homologous recombination was identified by PCR [64] using primers ARH-T 5'-ACGCTCGAGCAGCCCAAATCCATGCTATCCA TGGAC-3' and Neo-36 5'-CAGGACAGCAAGGGGGAGGATTGGGAAG AC-3' and confirmed by Southern blot analysis after *EcoR I* and *Sac I*

digestion, probing with *ARH* cDNA. Twelve independent stem cell clones containing a disrupted *Arh* allele were injected into C57Bl/6 blastocysts, yielding a total of 18 chimeric males. Of these 17 were fertile, and six gave offspring that carried the disrupted allele. Two separate lines were established for experimentation. No differences were detected between the two lines. Animals were genotyped by allele-specific PCR, using three primers. Primer ARH-T was used as the upstream oligo, while primers Neo-36 and ARH-GW 5'-CCTGTACTCCCAGACTACTTCATGATCCCCAC-3' were used as the downstream primers for the disrupted and wild-type alleles, respectively. Mice were housed on a 12-hour dark/12-hour light cycle, and given standard chow (no. 7002; Harlan Teklad, Madison, WI) and water *ad libitum*.

#### **Clearance of LDL, VLDL, $\alpha$ 2-macroglobulin, and asialofetuin from plasma –**

Clearance of lipoproteins,  $\alpha$ 2M, and asialofetuin was determined as previously described [54, 67]. Briefly, mice were anesthetized with sodium pentobarbital (80 mg/kg) and injected with a 0.2 ml intravenous bolus via the external jugular vein of either 15  $\mu$ g  $^{125}$ I-LDL, 15  $\mu$ g  $^{125}$ I-VLDL, 5  $\mu$ g  $^{125}$ I- $\alpha$ 2M, or 5  $\mu$ g  $^{125}$ I-asialofetuin in 10 mM Tris-HCl, pH 7.4, 150 mM NaCl, 0.2% (w/v) bovine serum albumin (BSA). At various time points

blood samples were drawn from the retro-orbital plexus into EDTA-coated tubes (Microvette 500 KE, Sarstedt, Newton, NC).  $^{125}\text{I}$ -labeled LDL and VLDL was measured by precipitating apoB with isopropanol followed by gamma counting. The plasma content of  $^{125}\text{I}$ - $\alpha$ 2M or  $^{125}\text{I}$ -asialofetuin was measured by trichloroacetic acid precipitation, followed by gamma counting. The amount of LDL, VLDL,  $\alpha$ 2M, or asialofetuin remaining in the blood was expressed as a percent of the initial blood concentration, measured as the average  $^{125}\text{I}$ -radioactivity in the plasma 2 min after injection.

#### **Measurement of VLDL production –**

Mice were fasted for 4 h at beginning of the light cycle. The mice were anesthetized with sodium pentobarbital (80 mg/kg) and injected in the external jugular vein with a bolus of 300 mg/kg Triton WR-1339 (Tyloxapol, Sigma, St. Louis, MO) in 0.9% NaCl (15% Triton WR-1339 w/v). Blood samples were collected into EDTA-coated tubes (Microvette 500 KE, Sarstedt, Newton, NC) from the retro-orbital plexus at the time points indicated. Total plasma volume was calculated as 3.15 ml/100 g body weight [68].

### **Interaction of ARH PTB domain with lipoprotein receptor tails –**

The LDLR family cytoplasmic tails/LexA fusion protein constructs and the mDab1 prey construct have been described previously [69]. The ARH-PTB domain was amplified from the cloned cDNA using the primers 5APY 5'-ATG**GAATTC**AGCCTCAAGTACCTTGGTATGACG-3' and 3APY 5'-TT**GTCGACT**CAGGACACCTGCCAAAACCTCAAAGGC-3'. The resulting PCR product was digested with *EcoR* I and *Sal* I, inserted into the *EcoR* I-*Xho* I digested prey vector pB42AD (MATCHMAKER system, Clontech, Palo Alto, CA), and sequenced. Yeast transformations and matings were performed following the manufacturer's instructions in the MATCHMAKER manual and interactions were assessed as previously described [69].

### **Localization of ARH and LDLR in mouse livers –**

Mice were sacrificed and perfused via cardiac puncture with warm Hank's balanced salt solution followed by 4% (w/v) paraformaldehyde (PFA) in PBS. The livers were removed and divided into 0.5 cm<sup>2</sup> sections. The tissue was fixed an additional hour at 25°C in 4% (w/v) PFA in PBS followed by an overnight incubation in 30% (w/v) sucrose solution. The tissue was frozen in OCT Compound 4583 (Miles Laboratories, Elkhart, IN) over dry ice and stored at -70°C until cutting. Sections of 7 µm were

cut on a Leitz Cryostat (E. Leitz, Inc., Rockleigh, NJ) at  $-20^{\circ}\text{C}$  and mounted onto poly-L-lysine coated slides. Samples were blocked by incubation for 1h with 10 mM Tris-HCl, pH 9.0, 150 mM NaCl (TBS) containing 20% (v/v) normal goat serum and 1% (w/v) BSA. Sections were then incubated overnight with rabbit antiserum raised against the PTB domain of ARH (1:800 dilution), rabbit antiserum against LRP [50] (1:200), or polyclonal rabbit IgG directed against the LDLR [51] (1:400). Slides were washed three times in TBS/0.1% BSA and bound primary antibody was detected by incubation for 2 h with 20  $\mu\text{g}/\text{ml}$  Alexa-Fluor 488-conjugated goat anti-rabbit IgG (Molecular Probes, Eugene, OR). Slides were washed three times in TBS/0.1% BSA, rinsed once with water, and mounted under a coverslip with Immu-mount (Shandon, Pittsburgh, PA). Images were acquired using the 63x0.70 objective on a Leica TCS-SP laser scanning confocal microscope.

### **Sucrose gradients –**

Male wild-type, *Arh*<sup>-/-</sup> and *Ldlr*<sup>-/-</sup> mice aged 15 weeks were fasted for 6 h and sacrificed. The livers were removed, rinsed briefly in cold PBS and minced in a weigh boat over ice. The minced liver was homogenized at 20% (w/v) in cold homogenization buffer (50 mM Tris-HCl, pH 7.4, 250 mM sucrose, 25 mM KCl, 5 mM MgCl<sub>2</sub>, 3 mM imidazole, Roche protease

inhibitor cocktail) with 20 strokes in a Dounce homogenizer. Nuclei and other debris were removed by low-speed centrifugation at 1000 *g* for 10 min at 4°C. 300 µl of the supernatant was loaded on a 4 ml continuous 10-40% sucrose gradient and centrifuged using a Beckman SW60 Ti rotor for 16 h at 40,000 rpm, as previously described [70]. A 20G needle was used to puncture the bottom of each tube and ~200 µl fractions were collected. Protein was precipitated with TCA, neutralized with NaOH, and dissolved in 100 µl sample buffer. A 10 µl aliquot was used for Western blotting.

### **Stimulation of cholesterol ester formation in peritoneal macrophage**

On Day 0 wild type, *Arh*<sup>-/-</sup>, and *Ldlr*<sup>-/-</sup> mice were given intraperitoneal injections of 2 ml 3.85% thioglycolate. On Day 4 the animals were sacrificed, and macrophage were collected by peritoneal lavage using cold PBS containing 200 µg/ml penicillin/200 µg/ml streptomycin. The cells were collected via low speed centrifugation and grown for 2 h at 37°C/5% CO<sub>2</sub> in DMEM, 10% LPDS, 100 µg/ml penicillin, 100 µg/ml streptomycin. The cells were then washed three times with PBS and grown an additional 36 h in DMEM, 10% LPDS, 100 µg/ml penicillin, 100 µg/ml streptomycin.

Cholesterol ester (CE) formation from [1-<sup>14</sup>C]oleate was determined

essentially as described [71]. Briefly, albumin bound [1-<sup>14</sup>C]oleate was added with rabbit  $\beta$ -VLDL at the concentrations indicated for 24 h. The cells were then washed at 4°C twice for 10 min with Buffer B (50 mM Tris-HCl, pH 7.4, 150 mM NaCl, 2 mg/ml BSA) and once briefly with Buffer C (50 mM Tris-HCl, pH 7.4, 150 mM NaCl). CE was extracted with hexane-isopropanol (3:2) to which <sup>3</sup>H-cholesteryl-oleate and unlabeled oleic acid were added as the internal standard and carrier, respectively. The organic phase was evaporated to dryness under flowing N<sub>2</sub>. Cholesterol [1-<sup>14</sup>C]-oleate was separated on silica coated TLC plates using a solvent system composed of heptane:ethyl ether:acetic acid (90:30:1; v:v:v), and its position was identified by staining with iodine vapor. The spots corresponding to CE were cut out and their radioactivities were quantified by liquid scintillation. Cellular protein was dissolved in 0.1 N NaOH and its concentration was determined by the Lowry method.

#### ***In vivo* complementation of ARH function in mice –**

To induce hypercholesterolemia, the *Arh*<sup>-/-</sup> mice (aged 12-16 weeks) were fed normal chow diets supplemented with 2% cholesterol/21% anhydrous milk fat for 3-5 weeks. On Day 0 the mice were anesthetized by intraperitoneal injection of sodium pentobarbital (100

µg/g body weight) and ~100 µl of blood was obtained via retro-orbital puncture. Recombinant adenovirus was then injected into the external jugular vein as a single dose ( $2 \times 10^{11}$  pfu in 200 µl of 10 mM Tris-HCl, pH 7.4, 150 mM NaCl, 2 mM MgCl<sub>2</sub>, 2 mM CaCl<sub>2</sub>, 0.2% (w/v) BSA) as described previously [72]. After recovery from anesthesia, mice were maintained on the cholesterol-enriched diet (see above) until Day 4 post-injection, when the animals were sacrificed. Since ARH expression from the recombinant adenovirus was sufficient to restore LDLR endocytosis in the *Arh*<sup>-/-</sup> mice without any addition of doxycycline, no doxycycline was supplied to the mice. Blood samples were drawn from the inferior vena cava for measurement of plasma cholesterol levels. The livers were removed and immunoblot analysis of ARH was performed on tissue lysates to confirm ARH expression.

### **Electron Microscopy –**

The tail veins of male mice aged 12-14 weeks were injected with 50 µg of LDL-gold or VLDL-gold. The animals were allowed to recover for 2 h, then sacrificed, and perfused with 4% paraformaldehyde in PBS via cardiac puncture. The livers were removed, diced and fixed with 2% glutaraldehyde and post-fixed in 1% (w/v) osmium tetroxide. Subsequently, the specimens were rinsed in distilled water, dehydrated

with graded ethanol and then Epon embedded according to the manufacturer's protocol (Electron Microscope Science). Ultrathin sections (~ 80 nm) were cut with a diamond knife using a Leica Ultracut R ultramicrotome and placed on Formvar/carbon-coated nickel grids. Ultrathin sections were stained with 3% aqueous uranyl acetate (15 min) and lead acetate (5 min). Electron micrographs were taken using a JEOL 1200 electron microscope operating at 80 kV.

#### **Uptake of fluorescent lipoproteins by primary hepatocytes –**

Primary hepatocytes were isolated from mice of the indicated genotypes as described with minor modifications [47]. Mice were anesthetized and the livers perfused via the portal vein with 30 ml of prewarmed Liver Perfusion Media (Invitrogen 17701-038, Carlsbad, CA) followed by 30 ml prewarmed Liver Digest Media (Invitrogen 17703-034) at ~3 ml/min. The livers were removed from the animals and Glisson's capsule was stripped. The dissociated cells were dispersed by shaking, followed by filtration through 100 µm nylon filter into an equal volume of cold Hepatocyte Wash Buffer (DMEM, 5% (v/v) FCS, 100 µg/ml penicillin, 100 µg/ml streptomycin, 10 mM HEPES, pH 7.4). The cells were washed two more times at 4°C with Hepatocyte Wash Buffer. The cells were counted with a hemacytometer and  $5 \times 10^5$  hepatocytes were plated onto

collagen I-coated coverslips (354089 BD Biosciences, Bedford, MA) in Hepatocyte Attachment Media (DMEM, 5% (v/v) lipoprotein-deficient serum, 100 µg/ml penicillin, 100 µg/ml streptomycin). The cells were incubated for 5 h at 37°C/5% CO<sub>2</sub>, after which the cells were washed with phosphate buffered saline (PBS), and incubated overnight in Hepatocyte Attachment Media at 37°C/5% CO<sub>2</sub>. The next morning 25 µg/ml PMCA-O LDL or 25 µg/ml Dil VLDL in Hepatocyte Attachment Media were added for the times indicated. The hepatocytes were then washed at 4°C twice for 10 min with Buffer B (50 mM Tris-HCl, pH 7.4, 150 mM NaCl, 2 mg/ml BSA) and once briefly with Buffer C (50 mM Tris-HCl, pH 7.4, 150 mM NaCl). The cells were then fixed with 4% paraformaldehyde (PFA) in Buffer F (20 mM sodium phosphate, pH 7.4, 150 mM NaCl, 2 mM MgCl<sub>2</sub>) at 25°C for 15 min. The cells were then briefly washed once with 50 mM NH<sub>4</sub>Cl, twice with Buffer F, and once with deionized H<sub>2</sub>O. Coverslips were mounted on slides with Immu-mount (Shandon, Pittsburgh, PA). Images were acquired using a Deltavision RT deconvolution microscope running *softWoRx* Explorer Suite 1.1 (Applied Precision, Issaquah, WA).

## **Internalization of monoclonal IgG and complexes by primary hepatocytes –**

Primary hepatocytes were isolated as described (see above). Hepatocytes were washed with cold PBS/1% BSA for 20 min and then incubated at 4°C for 1 h with 20 µg/ml IgG-C7 or IgG-2001 in Hepatocyte Attachment Media supplemented with 20 mM HEPES, pH 7.4. The cells were then warmed up to 37°C for the times indicated, after which the coverslips were washed twice for 10 min with ice cold Buffer B and once briefly with Buffer C. The cells were fixed for 15 min at 25°C with 4% PFA in Buffer F, then washed once in 50 mM NH<sub>4</sub>Cl, and once in Buffer F. The cells were permeablized for 10 min at -10°C with 0.05% (v/v) Triton X-100 in Buffer F. The cells were incubated for 1 h at 25°C in Blocking Solution (20 mM sodium phosphate, pH 7.4, 150 mM NaCl, 2 mM MgCl<sub>2</sub>, 10% (v/v) normal goat serum, 20 mg/ml BSA) and then for 2 h in 20 µg/ml Alexa-fluor 534 goat anti-mouse (Molecular Probes, Eugene, OR) in Blocking Solution. The cells were washed three times with 1 mg/ml BSA in Buffer F and once briefly in deionized water, before mounting. Images were acquired using 63x0.70 objective on Leica TCS-SP laser scanning confocal microscope. For experiments using IgG:Protein A complexes, the antibodies were pre-incubated at a 4:1 molar ratio with recombinant Protein A (21184 Pierce Biochemicals, Rockford, IL) for 1 h at room

temperature in buffer F. Complex formation was verified by blue-native PAGE [73].

## CHAPTER THREE

### GENERATION AND INITIAL CHARACTERIZATION OF ARH- DEFICIENT MICE

#### Overview

The limited available data from human subjects suggest that ARH function is tissue-specific, inasmuch as LDL internalization in ARH patients was found to be defective in the liver and in lymphoblasts [3], but is apparently largely normal in fibroblasts from the same patients [2]. Due to the inability to directly study the cell biological features of hepatocytes from affected humans, I generated an ARH deficient mouse by targeted gene disruption. These animals replicate central features of the human disease phenotype, including reduced clearance of LDL, hypercholesterolemia, and xanthomatosis. While the fractional removal of LDL was similar between *Arh*<sup>-/-</sup> mice and *Ldlr*<sup>-/-</sup> mice, the animal model for FH, *Arh*<sup>-/-</sup> animals replicated the less severe elevation in LDL-C seen in ARH patients compared to those with homozygous FH; however, LDL-C in the *Arh*<sup>-/-</sup> mice increased to similar levels as *Ldlr*<sup>-/-</sup> animals when challenged with fat and cholesterol enriched diets. Immunolocalization studies revealed that the LDLRs are isolated to sinusoidal surface of *Arh*<sup>-/-</sup> hepatocytes. ARH deficient mice remain the only physiological model

system in which the role of this specialized adaptor protein in receptor-mediated endocytosis can be experimentally investigated.

### **Generation of ARH deficient mice**

To disrupt the ARH allele in the mouse, I used targeted homologous recombination to replace exon 4 of *Arh* with a neomycin-resistance cassette [64] (Fig. 3-1A). Gene disruption was screened by PCR and confirmed by Southern blotting (Fig. 3-1B). Deletion of exon 4 disrupts the PTB domain and is predicted to render the protein unable to bind the NPXY motifs of LDLR family members. If splicing occurs between exons 3 and 5, a frame-shift and nonsense mutation would be introduced upstream of the putative binding sites for clathrin and AP-2 [37]. No immunoreactive ARH protein was detected in liver lysates of mice homozygous for the disruption using an antibody directed against the PTB domain (Fig. 3-1C). Levels of both LDLR and LRP protein were unchanged in the *Arh*<sup>-/-</sup> mice. *Arh*<sup>-/-</sup> mice were fertile and had normal litter sizes.

### **ARH deficient mice are hypercholesterolemic and exquisitely sensitivity to dietary cholesterol**

To determine whether the *Arh*<sup>-/-</sup> mice provided an experimental model that accurately replicated key phenotypic features of ARH in humans, I measured plasma cholesterol levels in wild type, *Arh*<sup>-/-</sup>, and *Ldlr*<sup>-/-</sup> mice. Plasma cholesterol levels were only mildly elevated (83 mg/dl) in the chow-fed *Arh*<sup>-/-</sup> mice compared to wild-type littermate controls (68 mg/dl) and significantly lower than and *Ldlr*<sup>-/-</sup> mice (196 mg/dl) (Table 3-1 and Fig. 3-2A). Since the plasma cholesterol levels in *Arh*<sup>-/-</sup>, *Arh*<sup>+/-</sup>, and wild type chow-fed animals were not significantly different, I challenged the mice with diets enriched with fat and cholesterol. Female *Arh*<sup>+/-</sup>, *Arh*<sup>-/-</sup>, *Ldlr*<sup>-/-</sup>, and wild-type mice were fed either chow supplemented with 0.2% cholesterol/21% fat (Western diet), or chow supplemented with 1.25% cholesterol/0.5% cholic acid/21% fat (Paigen diet) for 4 weeks. On the Western diet, plasma cholesterol levels were increased to a similar level in the *Arh*<sup>-/-</sup> and *Ldlr*<sup>-/-</sup> mice (Table 3-1 and Fig. 3-2A). Feeding of the Paigen diet resulted in dramatic elevations of plasma cholesterol levels to a mean of 1270 mg/dl for the *Arh*<sup>-/-</sup> mice and 1442 mg/dl for the *Ldlr*<sup>-/-</sup> mice. No significant differences were seen in plasma lipid levels between the *Arh*<sup>+/-</sup> mice and wild-type mice on any of the diets, which is consistent with the autosomal recessive inheritance pattern of ARH in humans. Liver

cholesterol and triglyceride levels were not significantly elevated in the *Arh*<sup>-/-</sup> mice over their wild-type or *Arh*<sup>+/-</sup> littermates (Table 3-1).

To determine the distribution of cholesterol in the lipoprotein fractions, pooled plasma from mice of the same genotype on the different diets was subjected to FPLC, as previously described [46, 47]. On the normal chow diet, little accumulation of LDL was observed in the *Arh*<sup>-/-</sup> animals (Fig. 3-2B). On the cholesterol-enriched diets, however, most of the cholesterol was found in the LDL fractions from the *Arh*<sup>-/-</sup> and *Ldlr*<sup>-/-</sup> mice (Fig. 3-2, C and D). The relative increase in LDL-C in the mice of different genotypes was estimated by taking the sum of the cholesterol content of each column fraction in the LDL peak. On the chow diet, LDL-C was increased 1.4-fold in the *Arh*<sup>-/-</sup> mice relative to wild-type littermates. Cholesterol feeding exacerbated this difference in the plasma cholesterol levels of these two genotypes. On a Western diet, the mean LDL-C level was 4.7-fold higher in the *Arh*<sup>-/-</sup> mice than in littermate controls and 7.3-fold higher than the *Arh*<sup>+/-</sup> mice on a chow diet. In contrast to these results, plasma LDL-C levels increased only 2-fold in *Ldlr*<sup>-/-</sup> mice fed the Western-type diet over their chow-fed counterparts.

Plasma LDL-C levels were increased 11-fold in the *Arh*<sup>-/-</sup> mice fed the Paigen diet when compared with wild-type littermates and 42-fold when compared with chow-fed *Arh*<sup>+/-</sup> mice. *Ldlr*<sup>-/-</sup> mice fed the Paigen

diet had LDL-C levels that were similar to those of *Arh*<sup>-/-</sup> mice on the same diet. LDL-C levels of *Ldlr*<sup>-/-</sup> animals were 12-fold increased over wild-type mice fed the same diet and 11-fold increased over *Ldlr*<sup>-/-</sup> mice that had been fed a 0.2% cholesterol-containing Western-diet. While dietary supplementation increased plasma cholesterol levels across all three genotypes, the hypercholesterolemia was exacerbated the most dramatically in the *Arh*<sup>-/-</sup> animals in response to cholesterol feeding.

**Clearance of <sup>125</sup>I-LDL but not <sup>125</sup>I- $\alpha$ 2M or <sup>125</sup>I-asialofetuin is reduced in *Arh*<sup>-/-</sup> mice**

Previous studies in humans suggested the FCR of LDL is reduced in ARH patients to a rate similar to that of patients with homozygous FH [2]. To determine the effect of ARH deficiency on hepatic LDLR function, I determined the rates of removal of <sup>125</sup>I-labeled LDL from the circulation of *Arh*<sup>-/-</sup>, wild-type and *Ldlr*<sup>-/-</sup> mice. The half-time for disappearance ( $t^{1/2}$ ) of <sup>125</sup>I-LDL was over twice as long in the *Arh*<sup>-/-</sup> mice as in wild-type animals (5.5 versus 2 h) (Fig. 3-3A). The rate of clearance of LDL from the circulation was as slow in the *Arh*<sup>-/-</sup> mice as in mice expressing no LDLR. To test whether the absence of ARH also impacted on the activity of other endocytic receptors in the liver, I examined the clearance of radiolabeled <sup>125</sup>I- $\alpha$ 2M and <sup>125</sup>I-asialofetuin. Asialofetuin is removed from the circulation

by the asialoglycoprotein receptor, a type II transmembrane receptor, whereas  $\alpha$ 2M is removed by LDLR family member, LRP. No differences were found between the rates of removal of  $^{125}\text{I}$ - $\alpha$ 2M or  $^{125}\text{I}$ -asialofetuin in the *Arh*<sup>-/-</sup> and wild-type mice (Fig. 3-3B-C).

#### **LDLR distribution is altered in the livers of *Arh*<sup>-/-</sup> mice –**

To determine the role of ARH on the subcellular distribution of the LDLR, I performed immunolocalization studies on liver sections from *Arh*<sup>-/-</sup>, *Ldlr*<sup>-/-</sup>, and wild-type mice using indirect immunofluorescence confocal microscopy. A diffuse cytoplasmic staining pattern was seen in sections from wild-type mice using a polyclonal anti-ARH antibody. Punctate ARH-specific staining was most intense at and immediately beneath the sinusoidal membrane. No differences in the pattern of ARH expression were seen in liver sections from the *Ldlr*<sup>-/-</sup> mice (Fig. 3-4A). Specific staining was absent from liver sections from *Arh*<sup>-/-</sup> mice and from sections to which the preimmune rabbit control serum had been applied (data not shown). LDLR distribution in the same liver sections was assessed using a rabbit polyclonal anti-mouse LDLR antibody. Cell surface staining as well as a predominant intracellular punctate staining in the cytoplasm was seen in the liver sections from wild-type mice.

A very different distribution of immunodetectable LDLR was seen in the *Arh*<sup>-/-</sup> mice. In the absence of ARH, LDLR was sequestered virtually exclusively to the sinusoidal membrane. To determine whether the absence of ARH affected the cellular location of other endocytic receptors, the distribution of LRP was examined. Consistent with normal  $\alpha$ 2M clearance in the *Arh*<sup>-/-</sup> mice, the subcellular distribution of LRP was not affected by the ARH disruption and indistinguishable among the liver sections from the *Arh*<sup>-/-</sup>, *Ldlr*<sup>-/-</sup>, and wild-type mice. Thus, absence of ARH specifically effected the distribution of the LDLR and was associated with a relative increase in cell surface staining.

### **Isopycnic Centrifugation of Liver Lysates on a Continuous Sucrose Gradient**

To determine the relative distribution of ARH and the LDLR within the various endocytic compartments in cells, analytical centrifugation was performed to fractionate vesicles from livers of *Arh*<sup>-/-</sup>, *Ldlr*<sup>-/-</sup>, and wild-type mice on a continuous sucrose gradient. The majority of ARH co-sedimented with vesicles containing early endosomal antigen 1 (EEA1) and rab5. Both proteins are associated with early endocytic compartments. Only a small percentage of ARH was present in the same fractions as the LDLR (Fig. 3-5). The distribution of ARH did not differ in

the absence or presence of the LDLR. These results are consistent with a subset of ARH being recruited to LDLR-containing early endocytic compartments independently of LDLR.

TABLE 3-1

## PLASMA CHOLESTEROL (mg/dl)

	0.02% Cholesterol	0.2% Cholesterol	1.25%Cholesterol/ 0.5% Cholic Acid
Wild type	67.7±8.1	125.9±38.5	184.9±35.8
<i>Arh</i> <sup>+/-</sup>	94.6±18.5	157.1±22.3	155.7±25.2
<i>Arh</i> <sup>-/-</sup>	83.1±7.9	307.9±62.9	1270.0±7.9
<i>Ldlr</i> <sup>-/-</sup>	196.4±7.6	239.1±80.5	1442.4±42.0

## LIVER TISSUE CHOLESTEROL (mg/g)

	0.02% Cholesterol	0.2% Cholesterol	1.25%Cholesterol/ 0.5% Cholic Acid
Wild type	2.64±0.05	6.80±1.73	19.58±0.75
<i>Arh</i> <sup>+/-</sup>	2.69±0.10	10.44±2.64	15.97±2.00
<i>Arh</i> <sup>-/-</sup>	2.67±0.15	6.76±0.75	23.23±0.21
<i>Ldlr</i> <sup>-/-</sup>	3.27±0.33	4.46±0.40	20.96±0.76

## PLASMA TRIGLYCERIDES (mg/dl)

	0.02% Cholesterol	0.2% Cholesterol	1.25%Cholesterol/ 0.5% Cholic Acid
Wild type	58.8±4.5	56.6±9.6	47.2±5.0
<i>Arh</i> <sup>+/-</sup>	56.2±9.3	61.4±6.5	46.2±1.8
<i>Arh</i> <sup>-/-</sup>	58.7±7.8	100.0±12.5	49.0±10.4
<i>Ldlr</i> <sup>-/-</sup>	97.4±12.1	94.8±22.7	129.2±1.4

## LIVER TISSUE TRIGLYCERIDES (mg/g)

	0.02% Cholesterol	0.2% Cholesterol	1.25%Cholesterol/ 0.5% Cholic Acid
Wild type	26.0±3.1	27.3±6.7	29.0±1.2
<i>Arh</i> <sup>+/-</sup>	22.3±7.5	33.5±2.4	19.9±7.0
<i>Arh</i> <sup>-/-</sup>	22.9±8.3	38.6±10.8	21.5±7.7
<i>Ldlr</i> <sup>-/-</sup>	26.4±6.1	36.3±11.1	11.3±0.7

Values are the mean cholesterol or triglyceride levels from three mice ± SEM

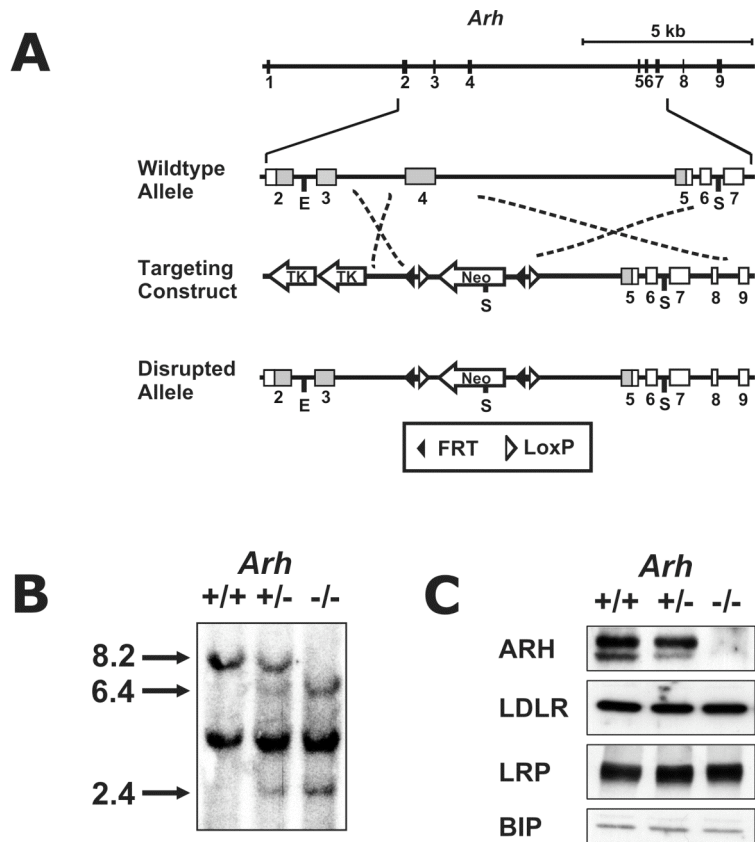


**Fig. 3-1** – Targeted disruption of the *Arh* gene. **A**, schematic structure of the mouse *Arh* gene locus and the knockout construct. The ARH PTB domain is encoded by exons 2–5, indicated by the *gray shading*. Homologous recombination resulted in the replacement of exon 4 with a PGK*neobpA* selection cassette [63], introducing a diagnostic *SacI* (S) restriction site. **B**, Southern blot of genomic DNA isolated from mouse tails of the indicated genotypes and digested with *EcoRI* (E) and *SacI* (S) and hybridized with the an ARH cDNA probe. An 8.2-kb band is generated from the wild-type allele, and a 2.4- and a 6.4-kb band are present in the disrupted allele due to the presence of a *SacI* site in *neo<sub>R</sub>*. **C**, immunoblot analysis of LDLR and LRP in ARH-deficient mice. Whole liver cell lysates were prepared as described [74], and 30  $\mu$ g of protein was fractionated using SDS-PAGE. Samples were analyzed by immunoblotting using antibodies against ARH, LDLR [51], and LRP [50]. Blots were stripped and incubated with antibodies to BiP (GRP78), which was used as a loading control.

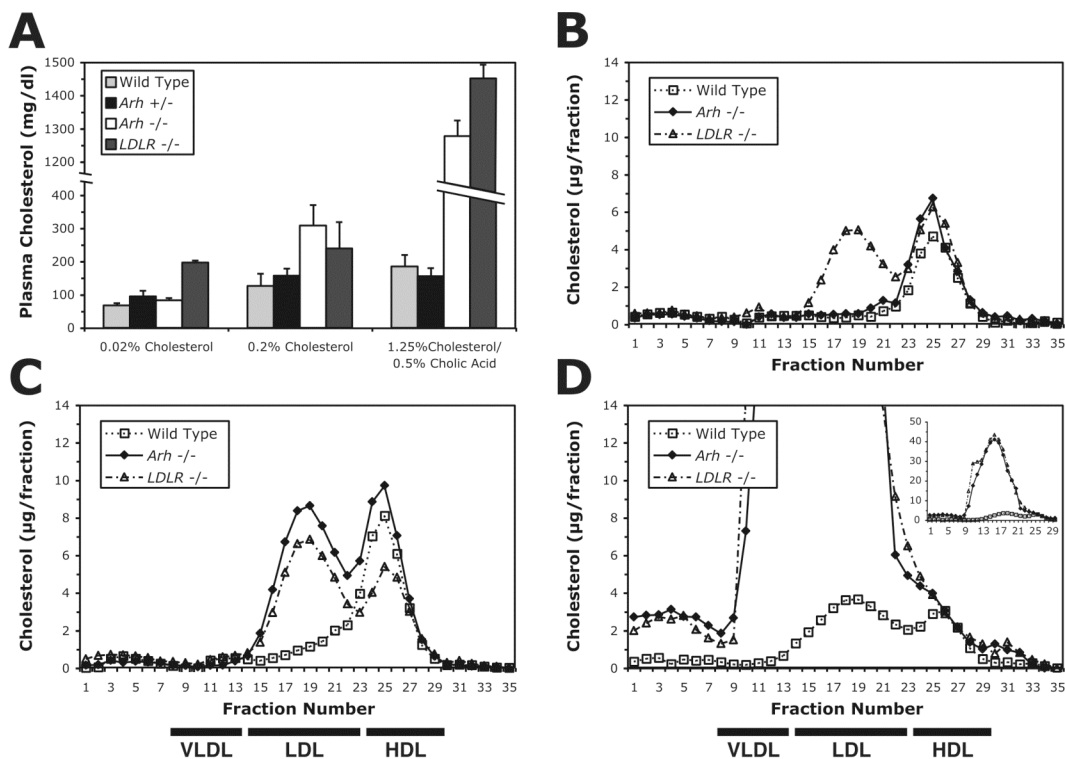


**Fig. 3-2.** Mean plasma cholesterol levels (**A**), and lipoprotein profiles (**B–D**) of *Arh*<sup>-/-</sup>, *Ldlr*<sup>-/-</sup>, and wild-type mice on chow and cholesterol-enriched diets. Female, 10–12-week-old *Arh*<sup>-/-</sup>, *Arh*<sup>+/-</sup>, and wild-type littermates and age-matched *Ldlr*<sup>-/-</sup> mice (four of each genotype) were fed a chow or cholesterol-enriched diet for 2 weeks. Plasma cholesterol levels were individually measured as described under “Methods.” Error bars represent S.E. **B–D**, fast protein liquid chromatography profiles of plasma lipoproteins. Wild-type (□), *Arh*<sup>-/-</sup> (◆), and *Ldlr*<sup>-/-</sup> (△) mice fed regular mouse chow containing 0.02% (w/w) cholesterol (**B**); chow supplemented with 0.2% (w/w) cholesterol (Western diet) (**C**); or chow supplemented with 1.25% (w/w) cholesterol (Paigen diet) (**D**). Mice were sacrificed after 2 weeks, and blood was collected from the inferior vena cava. Aliquots of plasma from the three animals in each group was pooled and subjected to FPLC gel filtration [46].

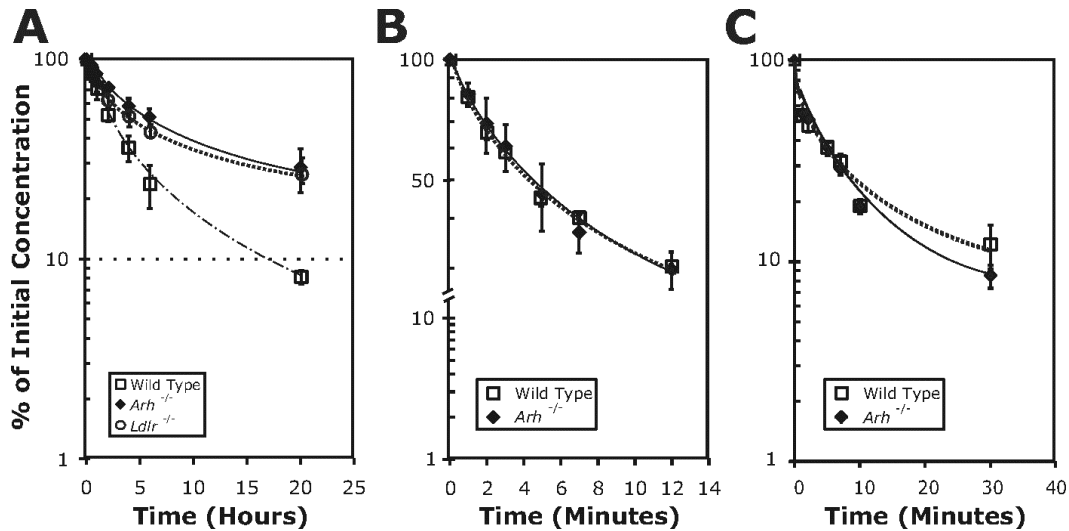


**Fig. 3-3** – Turnover of <sup>125</sup>I-labeled LDL, <sup>125</sup>I-α2M, and <sup>125</sup>I-asialofetuin in *Arh*<sup>-/-</sup>, *Ldlr*<sup>-/-</sup>, and wild-type mice. **A**, Four wild-type (□), *Arh*<sup>-/-</sup> (◆), and *Ldlr*<sup>-/-</sup> (△) 12–14-week-old male mice were injected in the external jugular vein with a bolus of 15 μg of <sup>125</sup>I-LDL (550 cpm/ng of protein). **B**, Three wild-type (□) and *Arh*<sup>-/-</sup> (◆) 12–14-week-old female mice were injected with 5 μg of <sup>125</sup>I-α2M (1250 cpm/ng). **C**, Three wild-type (□) and *Arh*<sup>-/-</sup> (◆) 12–14-week-old female mice were injected with 5 μg of <sup>125</sup>I-asialofetuin (1050 cpm/ng). Blood samples were collected by retro-orbital puncture at the indicated times, and the plasma content of trichloroacetic acid-precipitable <sup>125</sup>I-radioactivity was measured. Radioactivity remaining in the plasma was plotted as a percentage of the activity present 2 min after injection of the labeled ligand. Before the experiment, the mice were fasted for 6 h and anesthetized with sodium pentobarbital (80 mg/kg intraperitoneal).

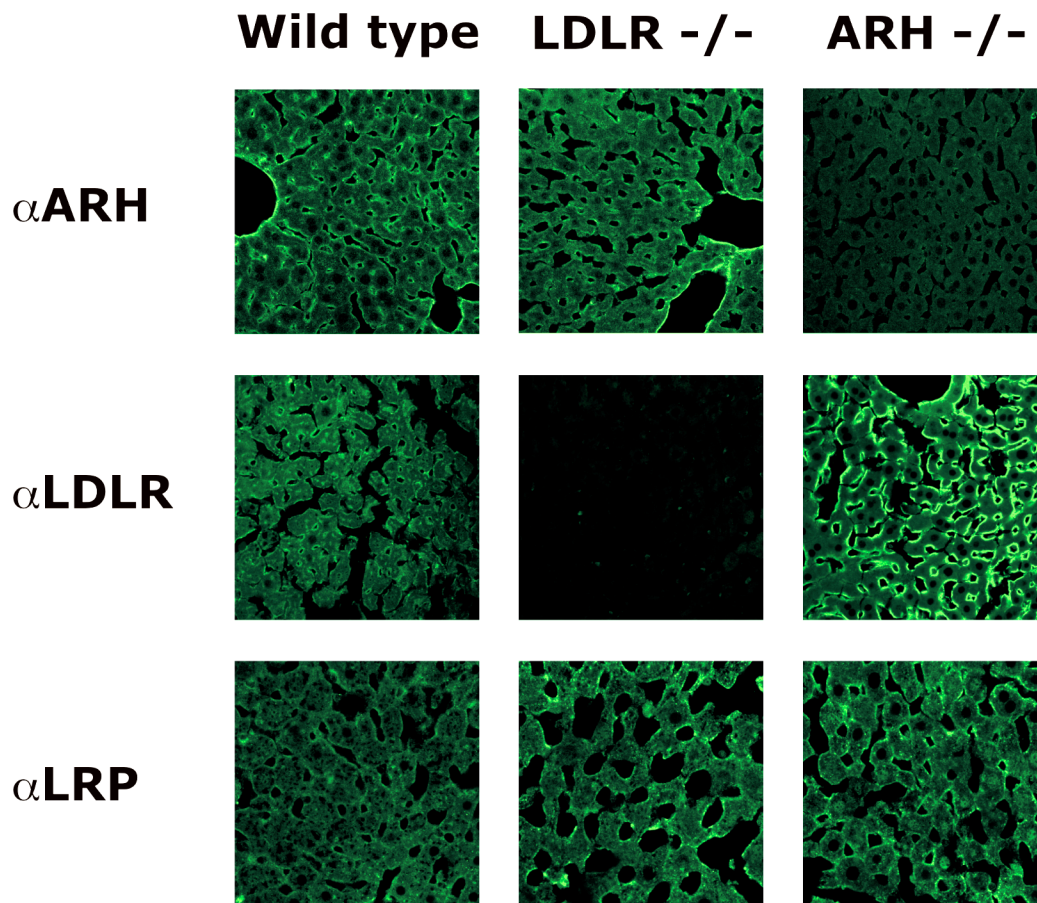


**Fig. 3-4** – Immunohistochemical staining of liver sections from wild-type, *Arh*<sup>-/-</sup>, *Ldlr*<sup>-/-</sup> mice. Frozen sections of liver from wild-type, *Arh*<sup>-/-</sup>, and *Ldlr*<sup>-/-</sup> mice were incubated with rabbit polyclonal antibodies against ARH, LDLR, and LRP. Bound IgG was detected with 20  $\mu$ g/ml Alexa-Fluor 488-labeled goat anti-rabbit IgG as described under “Methods.”

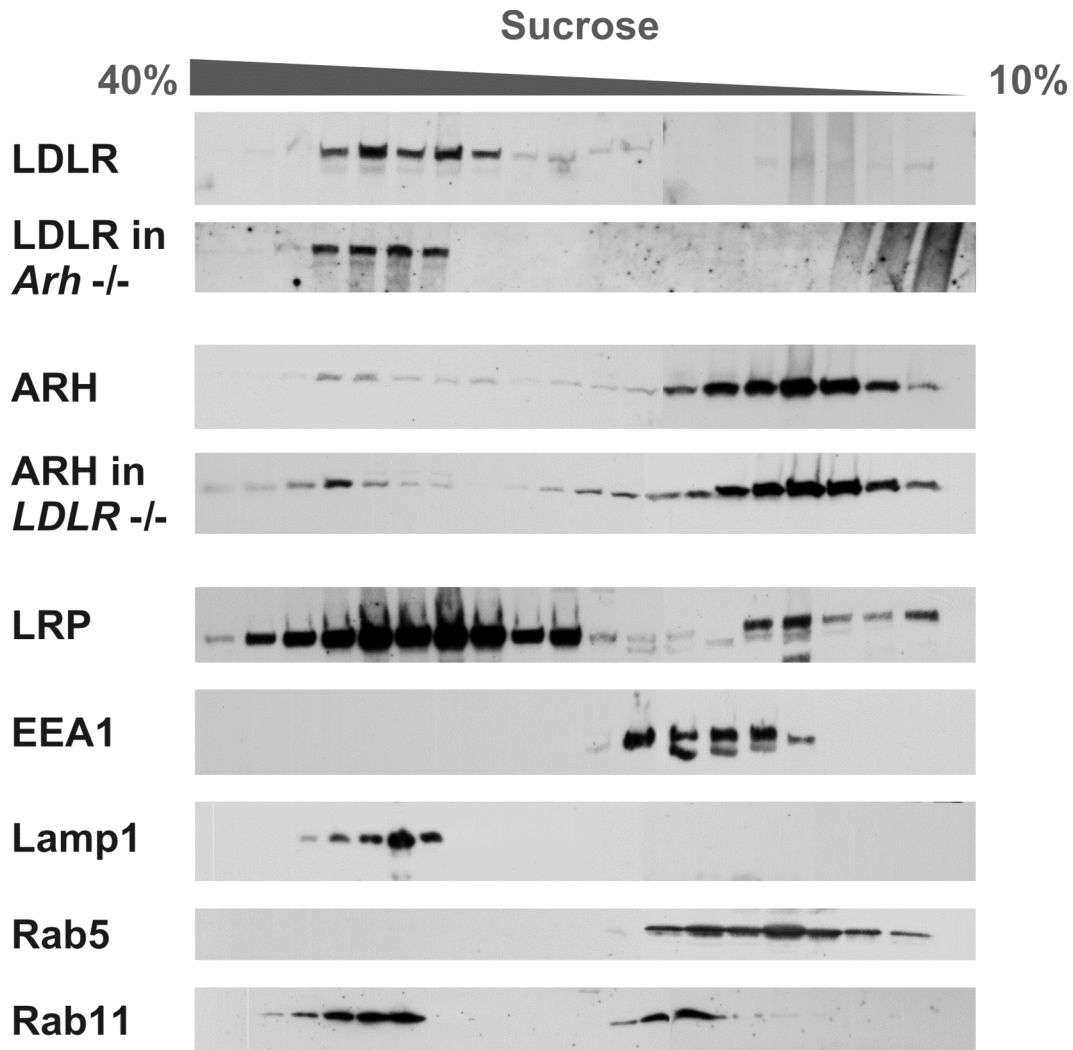


**Fig. 3-5** – Subcellular fractionation of ARH by isopycnic centrifugation on a continuous density gradient. Livers from 15-week-old male wild-type, *Arh*<sup>-/-</sup>, and *Ldlr*<sup>-/-</sup> mice were homogenized, and a postnuclear supernatant was loaded on top of a 10–40% continuous sucrose gradient. After centrifugation, fractions were collected, precipitated with trichloroacetic acid, and redissolved in 100  $\mu$ l of loading buffer. Proteins were separated by SDS-PAGE and analyzed by immunoblotting using antibodies against the respective proteins as described under “Methods.”

## CHAPTER FOUR

### ROLES OF ARH SUBDOMAINS

#### **Overview**

ARH is a modular adaptor protein with five regions highly conserved across vertebrates. Previous studies to determine the contribution of these domains to ARH function have involved *in vitro* binding assays to putative binding partners [37, 38]. From these assays the PTB domain was shown to bind both phosphoinositides and the peptide sequence FDNPVY in the LDLR cytoplasmic tail *in vitro*. A clathrin box sequence LLDLEE was shown to bind the clathrin heavy chain, and the conserved residues 248-275 in the human sequence was mapped as an interaction site for the  $\beta_2$  subunit of adaptin.

These studies, however, merely confirm binding partners predicted from the primary sequence. Due to sequence similarities between the cytoplasmic tails of the LDLR and other LDLR family members, ARH may play an as yet unrecognized role in the function of the LDLR family members. Binding partners and the relative importance in ARH function of the conserved N-terminal  $\alpha$ -helix and the putative type II PDZ domain binding site at the C-terminus cannot be easily predicted from the primary

sequence and have not as of yet been investigated. Additionally, *in vitro* interactions, however, fail to address the relative contributions of these domains singly or in combination to ARH function *in vivo*. In order to examine the contribution of these domains to ARH function, I designed an *in vivo* complementation assay using a tetracycline-responsive adenovirus expression system.

### **ARH Interacts with the Cytoplasmic Tails of Several LDLR Family**

#### **Members**

The cytoplasmic tail of each LDLR family member contains one or more characteristic NPXY motifs, to which the PTB domain of ARH is likely to bind. To identify other receptors with which ARH might interact, I performed yeast two-hybrid assay with a panel of LDLR family members. Surprisingly, in this assay ARH bound to the LDLR tail only relatively weakly but bound strongly to both splice variants of ApoER2 and also to the VLDL receptor. One possibility is the LDLR tail folds back upon itself and phosphorylation of serine 833 required for the cytoplasmic domain to take on a conformation amenable to ARH binding [75]. To test this hypothesis, I created both an LDLR tail with serine 833 replaced by aspartate (LDLR S833D) and a tail with a stop codon inserted after residue 829 (LDLR  $\Delta$ 829). This truncated LDLR has previously been

shown to undergo normal endocytosis [76]. Neither of these constructs demonstrated increased binding to ARH PTB domain (data not shown).

Since the NPXY motif in the cytoplasmic tails of both of these receptors is identical to that in the LDLR (Fig. 4-1), this finding suggests that the ARH PTB domain requires additional flanking amino acid residues for optimal binding. In addition, ARH was also capable of interacting with the first NPXY motif of megalin and the second NPXY motif of LRP. A paradigm for a receptor-specific role of PTB domain-containing adaptor proteins in endocytosis is also supported by the finding that Dab2, another PTB domain-containing protein that is most closely related to Dab1, binds to the cytoplasmic tail of megalin and is required for its endocytosis in the proximal tubule of the kidney [30].

### ***In vivo* complementation using ARH expressing adenovirus**

To examine the role of various ARH interaction sites on LDLR function *in vivo*, I used tetracycline-inducible recombinant adenoviruses to reconstitute hepatic ARH expression in *Arh*<sup>-/-</sup> mice (Fig. 4-2). Since chow fed *Arh*<sup>-/-</sup> mice are only mildly hypercholesterolemic, the mice were fed a high fat-high cholesterol diet (2% cholesterol/21% milk fat) for 3-5 weeks, resulting in a 4-7 fold increase in plasma cholesterol (375-700 mg/dl). Expression of wild-type human ARH in these mice was associated with a

reduction in circulating levels of plasma cholesterol, whereas no significant change in cholesterol levels occurred in mice expressing a control adenovirus (Fig. 4-3A,C). Expression of recombinant ARH partially restored ARH function in *Arh*<sup>-/-</sup> animals and ameliorated their hypercholesterolemia.

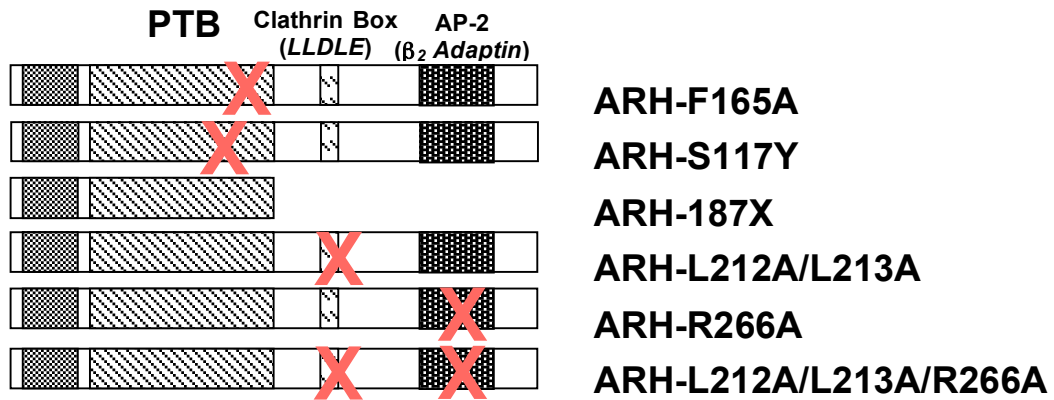
Previously, defined sequences within ARH were shown interact *in vitro* with the LDLR, the terminal domain of the heavy chain of clathrin, and  $\beta_2$ -adaptin, a subunit of AP-2 [37, 38]. To gauge the contribution of these individual domains to function of ARH, I tested a series of recombinant ARH constructs containing mutations predicted to disrupt binding to these other proteins. First, I tested two mutations predicted to disrupt the binding of the PTB domain to the LDLR. The first mutation substituted alanine for phenylalanine at residue 165 (F165A) in the PTB domain of ARH, a change that abolished binding of ARH to the LDLR *in vitro* [37]. Previously Stolt *et al.* showed that an identical mutation in the corresponding residue in another PTB domain-containing adaptor protein, Dab-1, only reduced the binding affinity of Dab1 for ApoER2, a member of the LDLR family by 10-fold, and an even greater reduction in affinity (70-fold) could be achieved by substituting tyrosine for serine at amino acid 114 [77, 78]. Therefore, I also tested a recombinant adenovirus with a substitution of serine for tyrosine (S117Y) at the corresponding residue of

the ARH PTB domain. Expression of recombinant ARH constructs containing either the ARH-F165A or the ARH-S117Y mutations in the PTB domain not only failed to lower plasma cholesterol levels, but also perhaps due to a dominant-negative effect actually exacerbated the hypercholesterolemia (Fig. 4-3C).

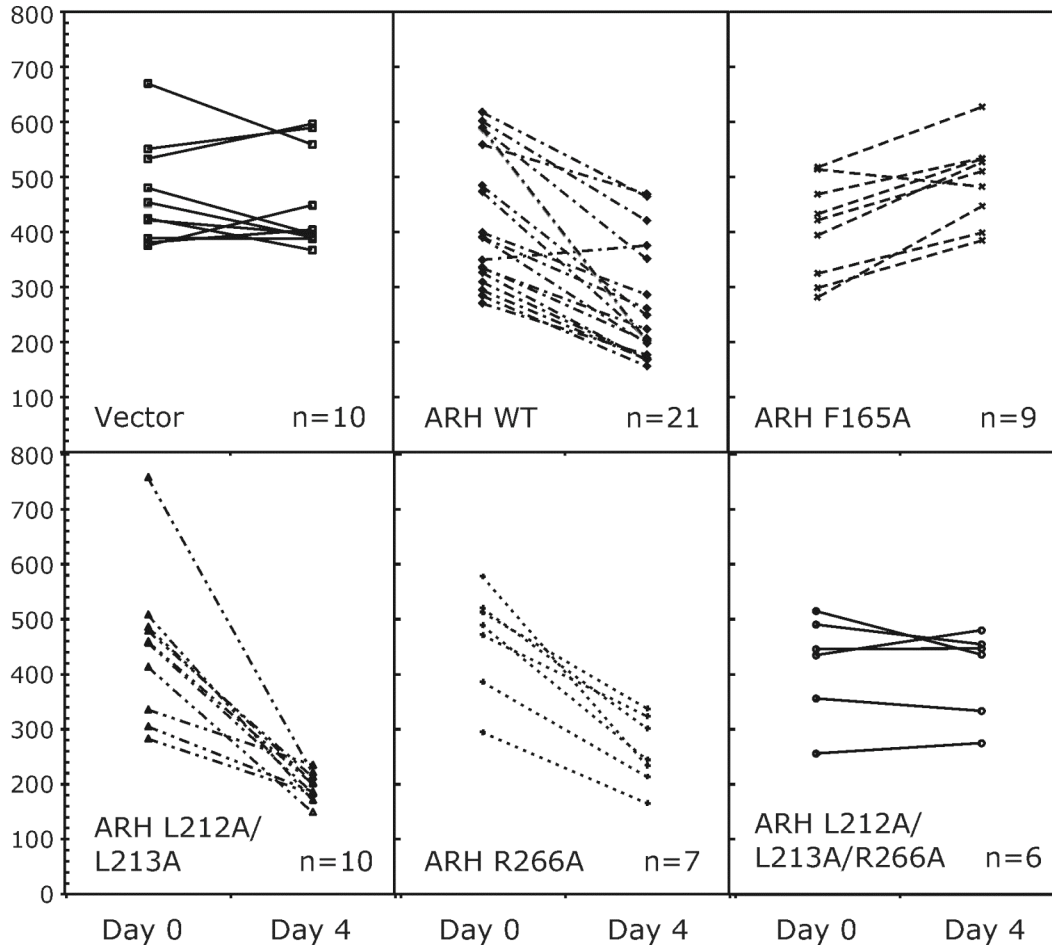
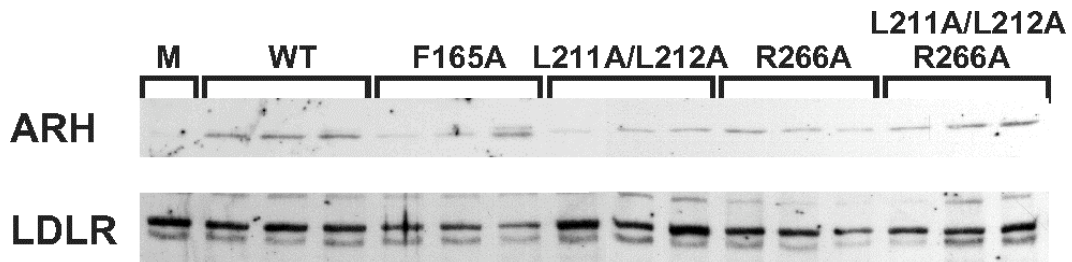
In contrast to these results, when recombinant ARH with mutations in either the clathrin box (AdARH-L212A/L213A) or in the AP-2 binding site (ARH-R266A) that disrupted binding *in vitro* [37] were expressed in the livers of the *Arh*<sup>-/-</sup> mice, the plasma levels of cholesterol fell to levels similar to mice infected with the wild-type ARH adenovirus. These results suggest that interactions between clathrin and AP-2 prevent the disruption of a single interaction between either partner and ARH from being sufficient to eliminate activity. To test this possibility, I injected *Arh*<sup>-/-</sup> mice with a recombinant adenovirus expressing both mutations (AdARH-L212A/L213A/R266A). No reduction in cholesterol level was seen in association with expression of an ARH with both the clathrin and AP-2 binding sites mutated.

Bait	Prey			Tail NPXY Sequences		
	ARH-PTB	Dab1 (pos. con.)	B42AD (neg. con.)			
LDLR	+	+++	-	-FDNPVY-		
LRP	+++	+++	++	-IGNPTY-	-FTNPVY-	
LRP A	-	-	-	-IGNPTY-		
LRP B	+++	+++	++	-IGNPTY-	-FTNPVY-	
Meg	+++	+++	-	-FENPMY-	-VDNKNY-	-FENPIY-
Meg A	+++	+++	-	-FENPMY-		
Meg B	-	-	-		-VDNKNY-	
Meg C	-	-	-			-FENPIY-
VLDLR	+++	+++	-	-FDNPVY-		
ApoER2+	+++	+++	-	-FDNPVY-		
ApoER2-	+++	+++	-	-FDNPVY-		
LexA	-	-	-			

**Fig 4-1** – Cytoplasmic tails of several LDLR family members interact with the ARH PTB domain. During the yeast mating assays clones containing bait, prey, and the reporter plasmid p8op-lacZ were selected on Trp-, Ura-, His-deficient plates. Four individual clones were transferred to patches on 5-bromo-4-chloro-3-indolyl  $\beta$ -D-galactopyranoside (X-gal) plates deficient in Trp, Ura, His, and Leu. Growth and blue staining was evaluated during 3 days at 30°C (no growth, -; weak to strong growth and staining +, ++, or +++). LRP and LRP B tails did show some degree of self-activation but allowed for some grading of the interaction. The (+) and (-) after the ApoER2 tail designate the presence of an alternatively spliced insert in the tail. The empty vectors (pLexA and pB42AD) were used as negative controls. Dab1 has previously been shown to interact with several LDLR family member tails and acted as a positive control.



**Fig. 4-2** – Adenoviral constructs expressing mutant ARH. Adenoviruses were created expressing ARH mutants that were predicted to disrupt association with LDLR (F165A and S117Y), clathrin (L212A/L213A), AP-2 (R266A), or both AP-2 and clathrin (187X and L212A/L213A/R266A).

**A****B**

C

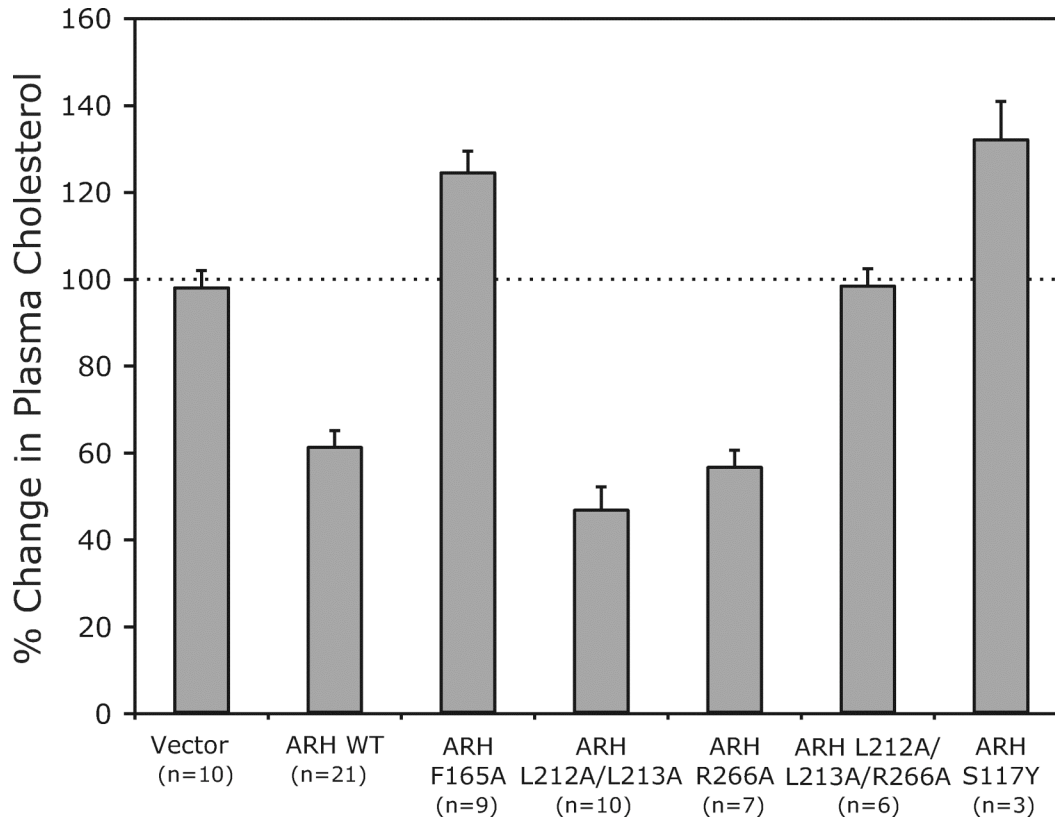


**Fig 4-3** – Reconstitution of ARH function in *Arh*<sup>-/-</sup> mice. Mice lacking ARH were fed chow diets supplemented with 2% cholesterol/21% anhydrous milk fat. After 3-5 weeks on the diet, blood samples for cholesterol determination were drawn from the retro-orbital plexus and the mice were injected with recombinant adenovirus ( $2 \times 10^{11}$  pfu) expressing wild-type or mutant ARH. Four days after injection the animals were sacrificed (A) plasma cholesterol levels of individual mice and (B) expression levels of the recombinant ARH proteins and LDLR were determined. (C) The effect of adenovirus administration on plasma cholesterol levels was calculated by dividing the value obtained on day 4 from the value obtained at baseline. The bars represent means  $\pm$  standard errors of the percent change in plasma cholesterol levels for each group of mice.

## CHAPTER FIVE

### XANTHOMATOSIS

#### Overview

When plasma cholesterol levels become severely elevated, LDL-C deposits in several tissues, in arterial walls (atheromas) and the skin and tendons (xanthomas). The rate of deposition in xanthomas is proportional to severity and duration of the elevation in plasma cholesterol in FH patients and will often occur in areas of local trauma [4]. Although individuals with ARH tend to have lower plasma LDL-C levels, xanthoma formation is often more extensive than seen in FH homozygotes with similar LDL-C levels. The substantial xanthomatosis observed in ARH has been hypothesized to result from preserved macrophage LDLR activity in macrophage, which may accelerate cholesterol accumulation in tendons and skin [6]. The only study directly measuring LDLR activity in ARH monocyte-derived macrophage found LDL internalization to be defective [9]. Here I examine whether *Arh*<sup>-/-</sup> mice are susceptible to xanthoma formation when placed on an atherogenic diet, and whether there are differences in the rates of cholesterol ester accumulation between macrophage harvested from *Arh*<sup>-/-</sup> and *Ldlr*<sup>-/-</sup> mice.

### **Xanthoma formation in *Arh*<sup>-/-</sup> mice**

To determine whether *Arh*<sup>-/-</sup> animals replicated the phenotype of humans with ARH by developing more extensive xanthomas than *Ldlr*<sup>-/-</sup> mice, I fed groups of wild type, *Arh*<sup>-/-</sup>, and *Ldlr*<sup>-/-</sup> mice normal chow supplemented for 14 months with 1.25% cholesterol/0.5% cholic acid/21% milkfat. Both *Arh*<sup>-/-</sup> and *Ldlr*<sup>-/-</sup> animals developed gross xanthomatous infiltration of the skin and subcutaneous tissue; however, the extent of deposition was essentially equivalent between the *Ldlr*<sup>-/-</sup> and *Arh*<sup>-/-</sup> mice (Fig 5-1B-C,E-F). Xanthomas appeared on both strains after similar time frames. Wild type mice remained completely free of xanthomas.

### **Cholesterol ester accumulation in *Arh*<sup>-/-</sup> macrophage**

Excess cholesterol taken up by macrophage is stored as cholesterol esters. Previously, Perrey, *et al.* demonstrated cholesterol ester formation is stimulated in the presence of VLDL but not LDL. The highest rate of cholesterol ester formation in macrophage was observed when LDLR be expressed by the macrophage and apoE must be present on the lipoprotein [57]. To determine whether VLDL could stimulate cholesterol ester formation in *Arh*<sup>-/-</sup> macrophage, I culture peritoneal macrophage from thioglycolate injected wild type, *Arh*<sup>+/-</sup>, *Arh*<sup>-/-</sup>, and *Ldlr*<sup>-/-</sup> mice. After the cultures were established, the macrophage were

incubated for 24 hours with increasing levels of rabbit  $\beta$ -VLDL. The *Arh*<sup>-/-</sup> macrophage accumulated cholesterol esters at a similar rate macrophage from *Arh*<sup>+/-</sup> and wild type mice (Fig. 5-2). Cholesterol ester formation was significantly retarded in macrophage from *Ldlr*<sup>-/-</sup> animals. These data suggest that independent of LDL internalization, *Arh*<sup>-/-</sup> macrophage may form foam cells more readily than *Ldlr*<sup>-/-</sup> macrophage in the presence of VLDL and may explain the increased susceptibility to xanthomatosis observed in ARH patients.

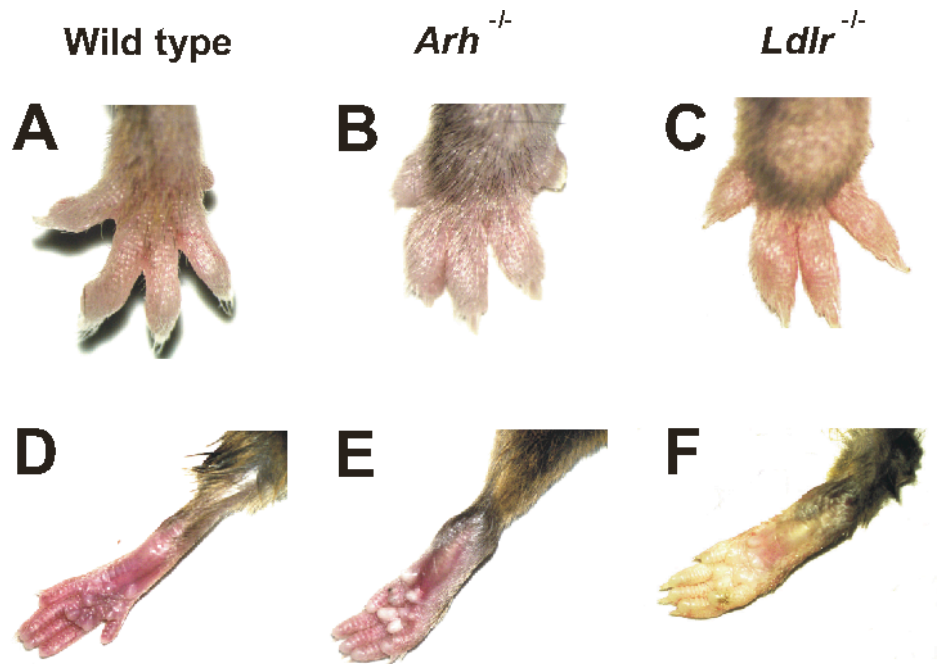


**Fig. 5-1** – Xanthomas in (**B-C,E-F**) *Arh*<sup>-/-</sup> and *Ldlr*<sup>-/-</sup> mice compared to xanthoma free (**A,D**) wild type mice. Mice were fed normal chow supplemented with 1.25% cholesterol/0.5% cholic acid/21% milk fat for 14 months. The tendons and skin of both *Arh*<sup>-/-</sup> and *Ldlr*<sup>-/-</sup> mice show extensive xanthomatous involvement.

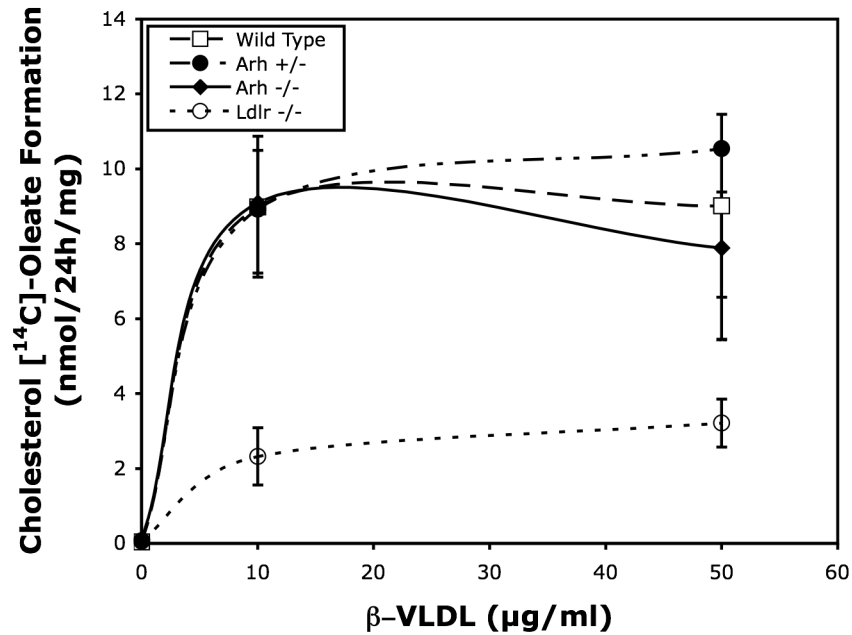


**Fig 5-2** – Cholesterol ester accumulation in cultured peritoneal macrophage from wild type, *Arh*<sup>+/-</sup>, *Arh*<sup>-/-</sup>, and *Ldlr*<sup>-/-</sup> mice. Thioglycolate stimulated macrophage were culture grown for 24 hours in LPDS followed by an additional 24 hours in the presence of the β-VLDL and <sup>14</sup>C-oleic acid. Cholesterol esters were separated by thin layer chromatography and quantified by scintillation counting.

## CHAPTER SIX

### VLDL METABOLISM IN ARH

#### Overview

Current evidence suggests the failure of LDLR internalization in the livers of ARH patients leads to their elevated levels of LDL. The question remains why this elevation in plasma cholesterol is less severe in patients with ARH than those patients with FH. This phenotype is replicated in *Arh*<sup>-/-</sup> mice, which only have moderately elevated cholesterol levels when fed a normal chow diet as compared to mice lacking LDLRs. One possible reason for the lower plasma cholesterol levels in *Arh*<sup>-/-</sup> mice could be a decreased production rate of VLDL compared to *Ldlr*<sup>-/-</sup> mice, leading to a smaller pool of VLDL remnants for conversion to LDL.

#### **Carbohydrate feeding leads to VLDL accumulation in *Ldlr*<sup>-/-</sup> but not *Arh*<sup>-/-</sup> mice**

To examine whether the mild hypercholesterolemia of *Arh*<sup>-/-</sup> could be exacerbated by increased VLDL synthesis, I fed *Arh*<sup>-/-</sup>, *Ldlr*<sup>-/-</sup> and wild type mice a high-carbohydrate diet for six weeks to increase the rate of hepatic VLDL production. As one might predict, carbohydrate feeding led to a marked accumulation of apoB-containing lipoproteins in the *Ldlr*<sup>-/-</sup>

mice, particularly as VLDL and IDL (Fig. 6-1). VLDL/IDL fractions were 136.4-fold enriched in cholesterol in *Ldlr*<sup>-/-</sup> compared to wild type animals, whereas LDL cholesterol was 20.4-fold elevated in the *Ldlr*<sup>-/-</sup> animals. Interestingly, *Arh*<sup>-/-</sup> mice failed to accumulate the high amounts of triglyceride-rich lipoproteins as *Ldlr*<sup>-/-</sup> animals. The most highly enriched fraction in the *Arh*<sup>-/-</sup> animals was in the form of LDL (5.3-fold over wild type mice).

#### **VLDL production rates are similar among wild type, *Ldlr*<sup>-/-</sup>, and *Arh*<sup>-/-</sup> mice**

While *Arh*<sup>-/-</sup> animals have previously been shown to be as defective at LDL clearance as *Ldlr*<sup>-/-</sup> mice, these results suggest that *Arh*<sup>-/-</sup> animals may be capable of removing VLDL and IDL from the circulation before conversion to LDL. An alternative explanation is that the presence of LDLR in the hepatocytes reduces the rate of secretion of VLDL through presecretory degradation [79]. To determine the rate of VLDL production in both chow-fed and carbohydrate-fed animals, I injected mice with the lipase inhibitor Triton WR-1339 and followed plasma triglyceride levels over time. Rates of production were similar among animals maintained on the same diet, though VLDL production rate was significantly increased in all animals fed a high-carbohydrate diet (Fig 6-2). These data suggest the

failure of *Arh*<sup>-/-</sup> mice to accumulate apoB-containing lipoproteins at levels comparable to *Ldlr*<sup>-/-</sup> mice is due to removal of particles from the circulation and not differences in the rate of VLDL production.

**VLDL is removed from the circulation of *Arh*<sup>-/-</sup> mice at an intermediate rate to *Ldlr*<sup>-/-</sup> and wild type mice**

ARH-deficient animals remove LDL from the circulation at a markedly reduced rate, which is similar to mice with no LDLRs. To determine whether *Arh*<sup>-/-</sup> animals are capable of clearing apoE-containing lipoproteins I injected the mice with <sup>125</sup>I-labeled mouse VLDL and the more easily obtainable <sup>125</sup>I-β-VLDL from cholesterol-fed rabbits and measured the remaining radioactivity in the plasma at various time points. VLDL is primarily cleared by the liver by the binding of apoE moieties on VLDL to LDLRs on the surface of hepatocytes. If LDLR internalization is completely defective in the livers of ARH animals, one would expect the rate of VLDL clearance to be similar between *Arh*<sup>-/-</sup> and *Ldlr*<sup>-/-</sup> mice. Interestingly, both mouse VLDL and rabbit β-VLDL were cleared at a rate faster than *Ldlr*<sup>-/-</sup> mice yet 3-fold slower than the wild-type mice (Fig 6-3B-C).

Future experiments required large amounts of LDL that would be impractical to obtain from mice; therefore, I opted to use human plasma as

a source of LDL. Since human LDL binds to the mouse LDLR poorly I employed mice with a human LDLR minigene inserted in the LDLR locus (*h*LDLR knock-in mice kindly provided by N. Maeda [55]). To determine whether the presence of the *h*LDLR would alter the uptake of lipoproteins from the plasma, I examined the clearance of  $^{125}\text{I}$ -*h*LDL and  $^{125}\text{I}$ - $\beta$ -VLDL in the *Ldlr*<sup>h/+</sup> animals on wild type and *Arh*<sup>-/-</sup> backgrounds. The *h*LDLR transcript is expressed at level 1.8-fold over the total transcript in wild type mice [55], so mice heterozygous for the *h*LDLR minigene were used. These animals gave similar results to mice without the *h*LDLR minigene (Fig 6-4).

#### **VLDL is cleared from the circulation by the liver *Arh*<sup>-/-</sup> mice**

To determine whether clearance of VLDL from the circulation was mediated by the liver in the *Arh*<sup>-/-</sup> animals, I examined the uptake of colloidal gold-labeled lipoproteins by the liver. Whereas both gold-labeled *h*LDL and  $\beta$ -VLDL were observed in endosomal compartments in the *Ldlr*<sup>h/h</sup> and wild type livers, respectively, only gold-labeled  $\beta$ -VLDL was detected inside the livers lacking ARH (Fig. 6-6). In *Arh*<sup>-/-</sup> *Ldlr*<sup>h/h</sup> livers the gold-labeled LDL was localized exclusively on the blood sinusoidal surface of the hepatocytes. Virtually no gold particles were observed in

hepatocytes of *Ldlr*<sup>-/-</sup> mice injected with either colloidal gold-labeled LDL or  $\beta$ -VLDL (data not shown).

### **VLDL but not LDL is internalized by *Arh*<sup>-/-</sup> hepatocytes**

To determine whether the differences observed in endocytosis of VLDL and LDL were intrinsic to the hepatocyte, primary hepatocytes were isolated from *Arh*<sup>+/+</sup> *Ldlr*<sup>h/h</sup>, *Arh*<sup>-/-</sup> *Ldlr*<sup>h/h</sup>, and *Ldlr*<sup>-/-</sup> mice and incubated with fluorescently labeled *h*LDL and  $\beta$ -VLDL. Both Dil  $\beta$ -VLDL and PMCA-O LDL were efficiently taken up by *Arh*<sup>+/+</sup> *Ldlr*<sup>h/h</sup> hepatocytes (Figure 6-7). Hepatocytes from the *Arh*<sup>-/-</sup> *Ldlr*<sup>h/h</sup> animals, however, only internalized Dil  $\beta$ -VLDL. Hepatocytes lacking LDLRs did not take up either lipoprotein.

### **Internalization of monoclonal IgG-C7 in hepatocytes –**

To determine whether the higher affinity of apoE over apoB for the LDLR was responsible for the preferential internalization of VLDL in *Arh*<sup>-/-</sup> hepatocytes, I tested whether ARH-deficient hepatocytes could take up the LDLR monoclonal antibody C7. IgG-C7 has a 2-4 fold higher affinity for LDLR than LDL [52]. Primary hepatocytes from *Arh*<sup>-/-</sup> *Ldlr*<sup>h/h</sup>, *Arh*<sup>+/+</sup> *Ldlr*<sup>h/h</sup>, and *Arh*<sup>+/+</sup> *Ldlr*<sup>-/-</sup> mice were incubated with IgG-C7 at 4°C for one hour and then warmed to 37°C for 2 hours. After the 4°C incubation LDLR is detected exclusively on the cell surface of *Arh*<sup>-/-</sup> *Ldlr*<sup>h/h</sup> and *Arh*<sup>+/+</sup> *Ldlr*

<sup>h/h</sup> hepatocytes (Fig. 6-8A). After warming the cells to 37°C, however, the IgG-C7 is redistributed from the surface to perinuclear vacuoles consistent with lysosomes in the *Arh*<sup>+/+</sup> *Ldlr*<sup>h/h</sup> hepatocytes. In contrast the IgG-C7 is retained at the cell surface in the *Arh*<sup>-/-</sup> *Ldlr*<sup>h/h</sup> hepatocytes. No specific staining was detected in the from *Arh*<sup>+/+</sup> *Ldlr*<sup>-/-</sup> cells (Fig 6-8A), or when using an irrelevant antibody, IgG-2001 (data not shown).

### **Receptor clustering is not sufficient to induce internalization in *Arh*<sup>-/-</sup> hepatocytes**

In addition to having a ~10-fold higher affinity for the LDLR than LDL, rabbit β-VLDL presents surface receptors with a multivalent ligand. To test whether clustering of LDLRs in the absence of ARH was sufficient to induce endocytosis, I formed tetramers of IgG-C7 with recombinant Protein A, which contains four high affinity Fc binding sites. The IgG-C7:Protein A tetramers were incubated with primary hepatocytes from *Arh*<sup>-/-</sup> *Ldlr*<sup>h/h</sup>, *Arh*<sup>+/+</sup> *Ldlr*<sup>h/h</sup>, and *Arh*<sup>+/+</sup> *Ldlr*<sup>-/-</sup> mice at 4°C for one hour and then warmed up to 37°C for 2 hours. After 1 hour at 4°C the IgG-C7:Protein A was detected on the cell surface of *Arh*<sup>-/-</sup> *Ldlr*<sup>h/h</sup> and *Arh*<sup>+/+</sup> *Ldlr*<sup>h/h</sup> hepatocytes (Fig. 6-8B). After warming the cells to 37°C, IgG-C7:Protein A was internalized only by the *Arh*<sup>+/+</sup> *Ldlr*<sup>h/h</sup> hepatocytes. All of the IgG-C7:Protein A complexes remained on the cell surface in the

*Arh*<sup>-/-</sup> *Ldlr*<sup>h/h</sup> hepatocytes. No staining was seen in the *Arh*<sup>+/+</sup> *Ldlr*<sup>-/-</sup> hepatocytes (Fig. 6-8B) or when IgG-2001:Protein A complexes were used (data not shown).

**LDLR-related protein is not required for  $\beta$ -VLDL uptake by *Arh*<sup>-/-</sup> hepatocytes.**

It is also possible that the LDLR binds VLDL and then transfers it to or forms a complex with a second receptor on the cell surface, such as the LDLR-related protein (LRP), for internalization. In this model, an alternative adaptor that recognizes the cytoplasmic tail of LRP could mediate internalization of the complex, obviating the requirement for ARH. To test this hypothesis, we examined the effects of LRP deletion on  $\beta$ -VLDL uptake in ARH-deficient animals. Mice lacking ARH were crossed with mice containing loxP sites at the LRP locus [39, 80] to generate *Arh*<sup>-/-</sup> *Lrp*<sup>lox/lox</sup> animals. LRP was selectively deleted in the livers of these animals by introduction of a transgene expressing Cre recombinase (*Arh*<sup>-/-</sup> *Lrp*<sup>lox/lox</sup> *Cre*<sup>+</sup>) under the control of the albumin promoter [81]. Deletion of LRP markedly impaired clearance of  $\alpha$ 2-macroglobulin, an established ligand for LRP, but did not affect clearance of VLDL remnants in *Arh*<sup>-/-</sup> animals. Primary hepatocytes from *Arh*<sup>-/-</sup> *Lrp*<sup>lox/lox</sup> *Cre*<sup>-</sup> mice internalized both  $\beta$ -VLDL and  $\alpha$ 2-macroglobulin (Figure 6-9). Deletion of LRP in these

cells did not reduce the uptake of  $\beta$ -VLDL despite abolishing the internalization of  $\alpha$ 2-macroglobulin. These findings indicate that the LDLR-dependent internalization of  $\beta$ -VLDL in *Arh*<sup>-/-</sup> hepatocytes does not require LRP.

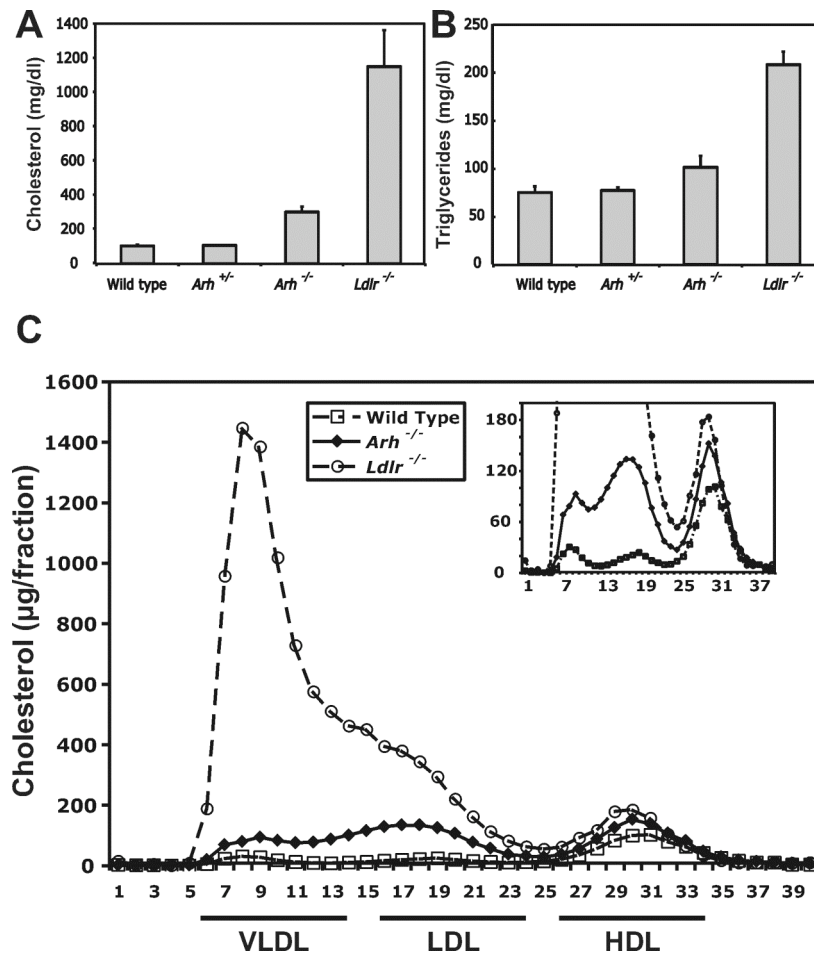
TABLE 6-1

Genotype	Plasma Cholesterol (mg/dl)	Plasma Triglycerides (mg/dl)
Wild Type	102.7 ± 8.7	75.0 ± 6.8
<i>Arh</i> <sup>+/-</sup>	106.1 ± 4.6	77.2 ± 3.4
<i>Arh</i> <sup>-/-</sup>	301.0 ± 33.9	101.2 ± 12.3
<i>Ldlr</i> <sup>-/-</sup>	1147.8 ± 214.0	208.1 ± 13.8

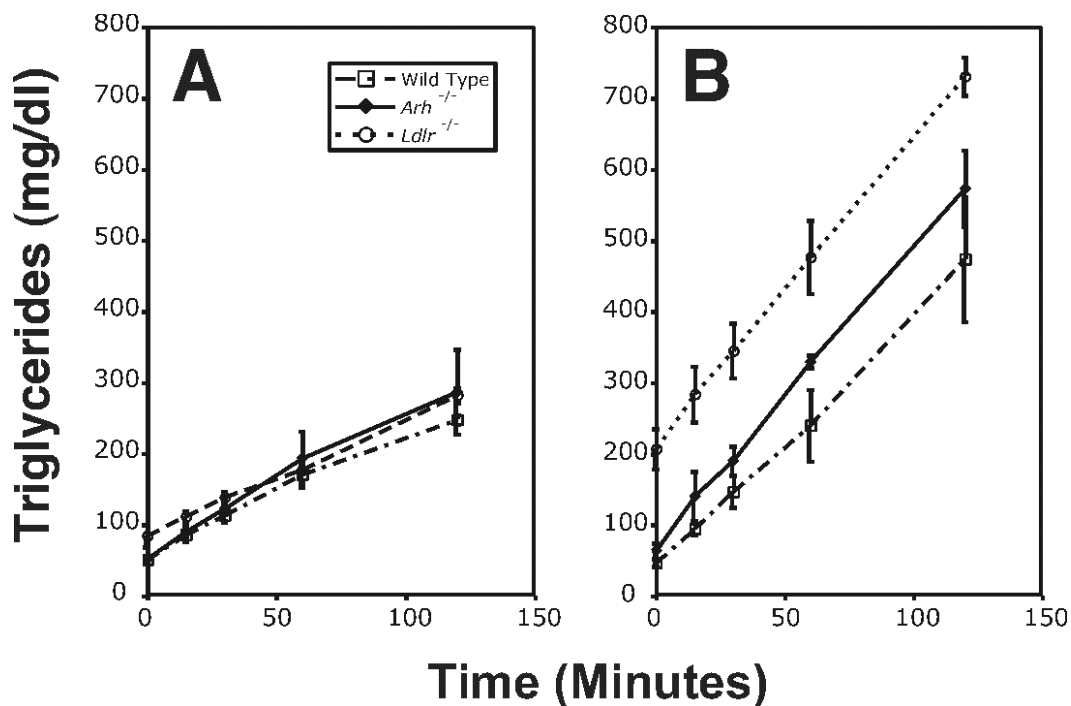
  

Genotype	Liver Cholesterol (mg/g)	Liver Triglycerides (mg/g)
Wild Type	5.54 ± 1.26	32.6 ± 5.5
<i>Arh</i> <sup>+/-</sup>	5.95 ± 4.6	33.7 ± 9.1
<i>Arh</i> <sup>-/-</sup>	6.31 ± 1.26	26.8 ± 6.0
<i>Ldlr</i> <sup>-/-</sup>	8.97 ± 1.19	27.2 ± 0.8

Cholesterol and triglyceride content in the plasma and liver of mice fed a high-carbohydrate diet for 6 weeks. Values are the mean cholesterol or triglyceride levels from five mice ± SEM



**Fig. 6-1.** Mean plasma cholesterol and triglyceride levels (**A-B**), and lipoprotein profiles (**C**) of *Arh*<sup>-/-</sup>, *Ldlr*<sup>-/-</sup>, and wild-type mice fed carbohydrate-enriched diets. **A-B**, Female, 12–16-week-old *Arh*<sup>-/-</sup>, *Arh*<sup>+/-</sup>, and wild-type littermates and age-matched *Ldlr*<sup>-/-</sup> mice (six of each genotype) were fed a high-carbohydrate diet for 6 weeks. Plasma cholesterol and triglyceride levels were individually measured as described under “Methods.” *Error bars* represent S.E. **C**, fast protein liquid chromatography profiles of plasma lipoproteins. Wild-type (□), *Arh*<sup>-/-</sup> (◆), and *Ldlr*<sup>-/-</sup> (○) mice fed a diet containing 60.2% sucrose, 20% casein, 15% cellulose, 0.3% DL-methionine, 3.5% minerals and vitamins, and <0.2% fat. Mice were sacrificed after 6 weeks, and blood was collected from the inferior vena cava. Aliquots of plasma from the animals in each group was pooled and subjected to FPLC gel filtration [46].



**Fig. 6-2** – VLDL production rates in (A) chow-fed and (B) carbohydrate-fed *Arh*<sup>-/-</sup>, *Ldlr*<sup>-/-</sup>, and wild-type mice. Four male wild-type (□), *Arh*<sup>-/-</sup> (◆), and *Ldlr*<sup>-/-</sup> (○) mice, age 14-16 weeks, were maintained for six weeks on either (A) normal chow containing 6% fat/0.02% cholesterol or (B) a diet comprised of 60.2% sucrose, 20% casein, 15% cellulose, 0.3% DL-methionine, 3.5% minerals and vitamins, and <0.2% fat. At the end of six weeks the animals were injected with 300 mg/kg Triton WR-1339 and blood was sampled via retro-orbital venupuncture at the times indicated. Plasma triglyceride content was measured as described under “Methods.” Error bars represent S.E.

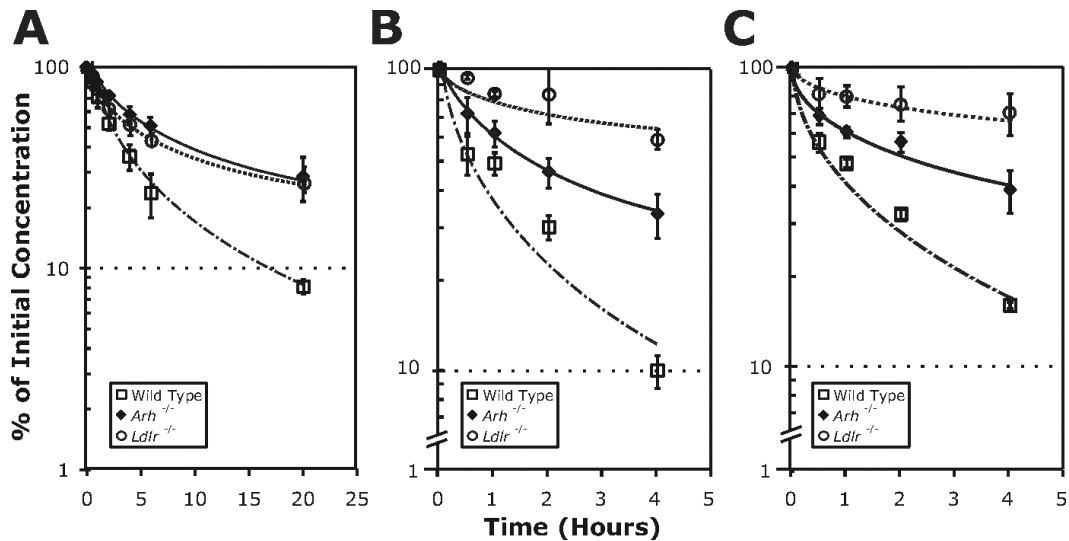


**Fig. 6-3** – Clearance of  $^{125}\text{I}$ -labeled mouse LDL, mouse  $^{125}\text{I}$ -VLDL, and rabbit  $^{125}\text{I}$ - $\beta$ -VLDL in *Arh*<sup>-/-</sup>, *Ldlr*<sup>-/-</sup>, and wild-type mice. **A**, Four wild-type ( $\square$ ), *Arh*<sup>-/-</sup> ( $\blacklozenge$ ), and *Ldlr*<sup>-/-</sup> ( $\circ$ ) 12–14-week-old male mice were injected in the external jugular vein with a bolus of 15  $\mu\text{g}$  of  $^{125}\text{I}$ -LDL (550 cpm/ng of protein). **B**, Four wild-type ( $\square$ ), *Arh*<sup>-/-</sup> ( $\blacklozenge$ ), and *Ldlr*<sup>-/-</sup> ( $\circ$ ) 12–14-week-old female mice were injected with 15  $\mu\text{g}$  of  $^{125}\text{I}$ -VLDL (125 cpm/ng). **C**, Four wild-type ( $\square$ ), *Arh*<sup>-/-</sup> ( $\blacklozenge$ ), and *Ldlr*<sup>-/-</sup> ( $\circ$ ) 12–14-week-old female mice were injected with 15  $\mu\text{g}$  of rabbit  $^{125}\text{I}$ - $\beta$ -VLDL (288 cpm/ng). Blood samples were collected by retro-orbital puncture at the indicated times, and the plasma content of isopropanol-precipitable  $^{125}\text{I}$ -radioactivity was measured. Radioactivity remaining in the plasma was plotted as a percentage of the activity present 2 min after injection of the labeled ligand. Before the experiment, the mice were fasted for 6 h and anesthetized with sodium pentobarbital (80 mg/kg intraperitoneal).

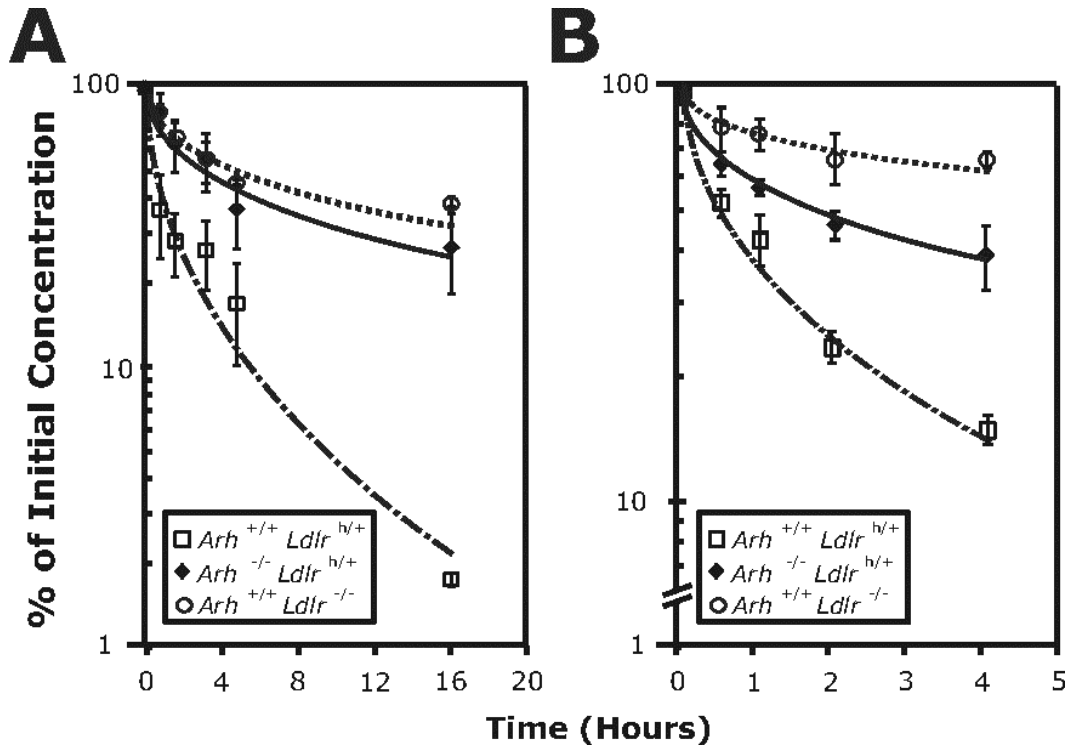


**Fig. 6-4** – Clearance of <sup>125</sup>I-labeled human LDL and rabbit <sup>125</sup>I-β-VLDL in *Arh*<sup>-/-</sup> *Ldlr*<sup>h/h</sup>, *Arh*<sup>+/+</sup> *Ldlr*<sup>h/h</sup>, and *Arh*<sup>+/+</sup> *Ldlr*<sup>-/-</sup> mice. **A**, Four *Arh*<sup>+/+</sup> *Ldlr*<sup>h/h</sup> (□), *Arh*<sup>-/-</sup> *Ldlr*<sup>h/h</sup> (◆), and *Arh*<sup>+/+</sup> *Ldlr*<sup>-/-</sup> (○) 10–12-week-old female mice were injected in the external jugular vein with a bolus of 15 μg of human <sup>125</sup>I-LDL (125 cpm/ng of protein). **B**, Four *Arh*<sup>+/+</sup> *Ldlr*<sup>h/h</sup> (□), *Arh*<sup>-/-</sup> *Ldlr*<sup>h/h</sup> (◆), and *Arh*<sup>+/+</sup> *Ldlr*<sup>-/-</sup> (○) 10–12-week-old female mice were injected with 15 μg of rabbit <sup>125</sup>I-β-VLDL (288 cpm/ng). Blood samples were collected by retro-orbital puncture at the indicated times, and the plasma content of isopropanol-precipitable <sup>125</sup>I-radioactivity was measured. Radioactivity remaining in the plasma was plotted as a percentage of the activity present 2 min after injection of the labeled ligand. Before the experiment, the mice were fasted for 6 h and anesthetized with sodium pentobarbital (80 mg/kg intraperitoneal).

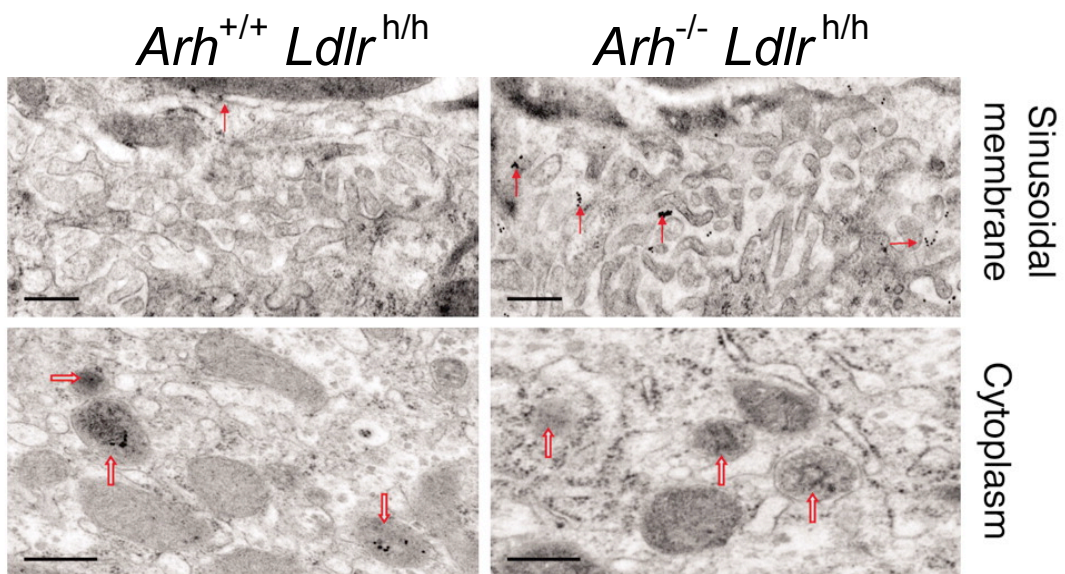
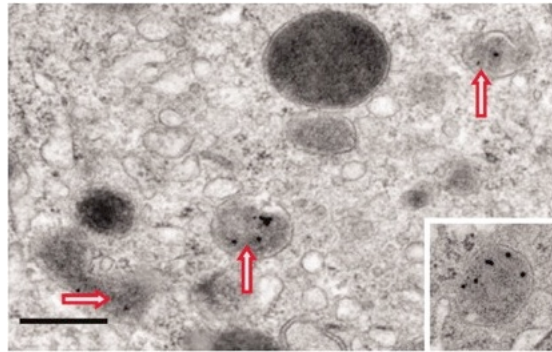
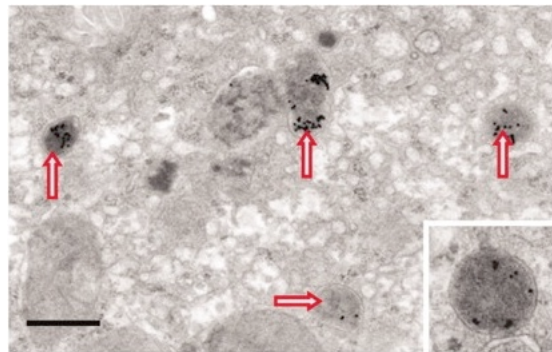


**Fig 6-5** – Electron micrographs of LDL-gold in livers from *Arh*<sup>+/+</sup> *Ldlr*<sup>h/h</sup> and *Arh*<sup>-/-</sup> *Ldlr*<sup>h/h</sup> mice. Male *Arh*<sup>+/+</sup> *Ldlr*<sup>h/h</sup> and *Arh*<sup>-/-</sup> *Ldlr*<sup>h/h</sup> mice, age 12-14 weeks, were injected via the tail vein with 50 µg of colloidal gold-labeled human LDL. After 2 h the animals were sacrificed and the livers removed. LDL-gold was detected by electron microscopy as described in “Methods.” Solid arrows indicate gold particles associated with villi on the sinusoidal membrane, and open arrows indicate endosomes. Scale bars: 0.5 µm.

Wild Type



*Arh*<sup>-/-</sup>



*Ldlr*<sup>-/-</sup>

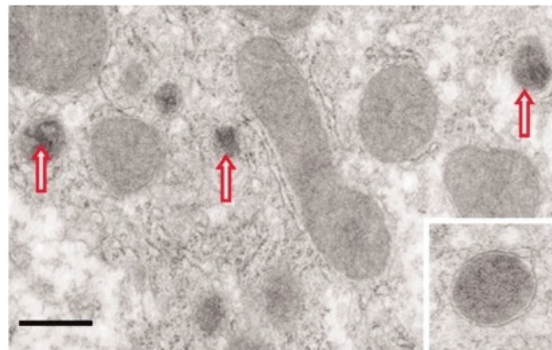


**Fig 6-6** – Electron micrographs of  $\beta$ -VLDL-gold in livers from wild type, *Arh*<sup>-/-</sup>, and *Ldlr*<sup>-/-</sup> mice. Male wild type, *Arh*<sup>-/-</sup>, and *Ldlr*<sup>-/-</sup> mice, age 12-14 weeks, were injected via the tail vein with 50  $\mu$ g of colloidal gold-labeled rabbit  $\beta$ -VLDL. After 2 h the animals were sacrificed and the livers removed.  $\beta$ -VLDL-gold was detected by electron microscopy as described in “Methods”. Open arrows indicate endosomes. Scale bars: 0.5  $\mu$ m.

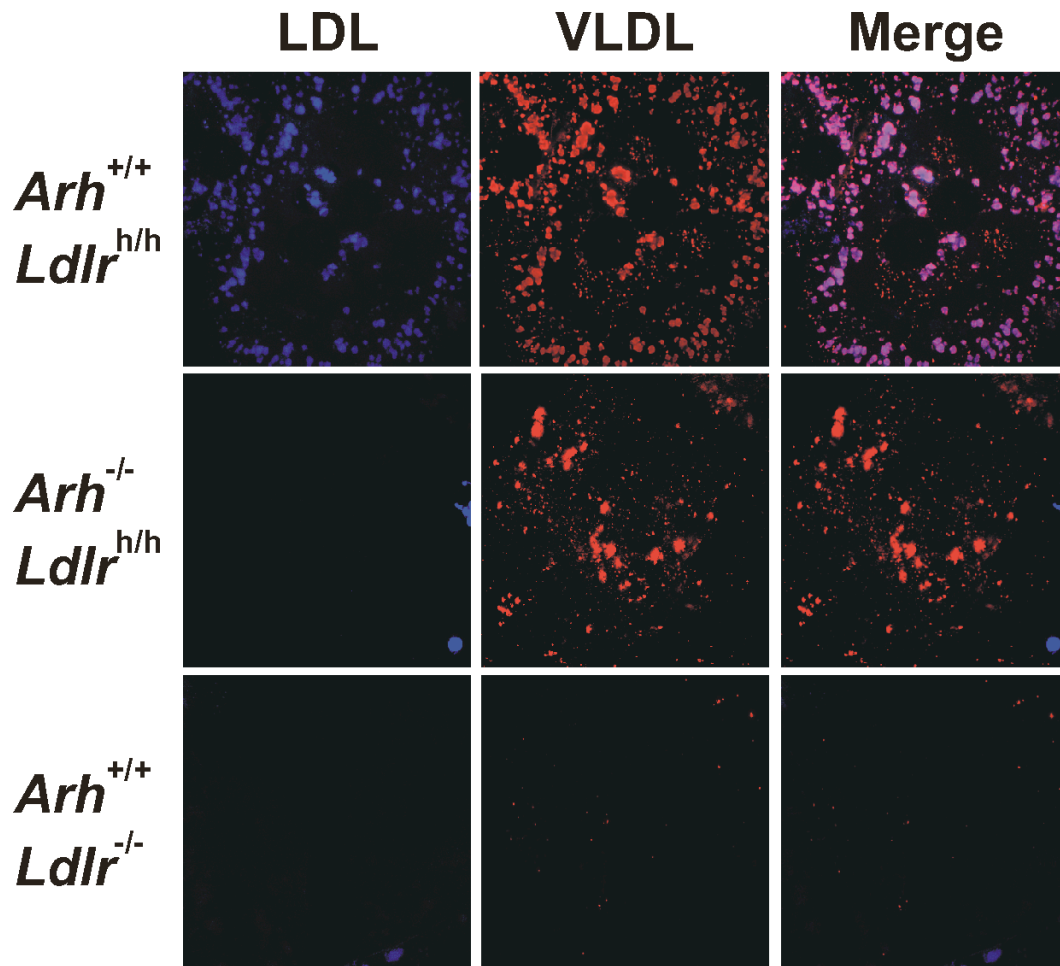


**Fig 6-7** – Internalization of fluorescent lipoproteins by primary hepatocytes. Primary hepatocytes were isolated from *Arh*<sup>+/+</sup> *Ldlr*<sup>h/h</sup>, *Arh*<sup>-/-</sup> *Ldlr*<sup>h/h</sup> and *Arh*<sup>+/+</sup> *Ldlr*<sup>-/-</sup> mice and grown overnight on collagen I-coated coverslips. The next morning the cells were incubated with 25  $\mu$ g PMCA-O LDL (blue) and 25  $\mu$ g Dil  $\beta$ -VLDL (red) for 5 hours, fixed, and immediately visualized by deconvolution microscopy.

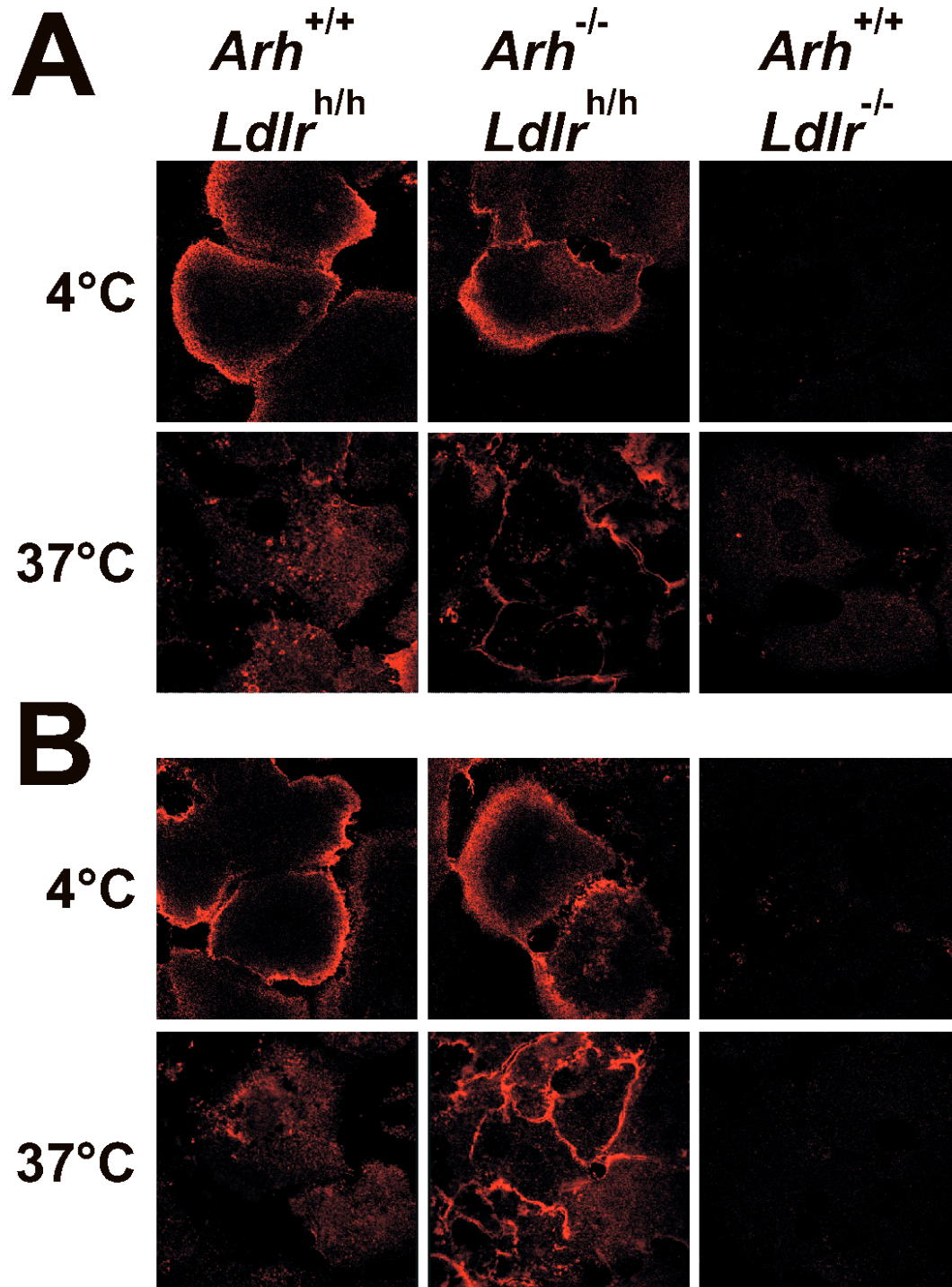


**Fig. 6-8** – Internalization of IgG-C7 and IgG-C7:Protein A complexes in primary hepatocytes. Primary hepatocytes were isolated from *Arh*<sup>+/+</sup> *Ldlr*<sup>h/h</sup>, *Arh*<sup>-/-</sup> *Ldlr*<sup>h/h</sup> and *Arh*<sup>+/+</sup> *Ldlr*<sup>-/-</sup> mice and incubated for 1 h at 4°C with either (**A**) IgG-C7 or (**B**) IgG-C7 complexed with Protein A. The cells were then warmed to 37°C for two hours. IgG-C7 was detected by indirect immunofluorescent confocal microscopy.

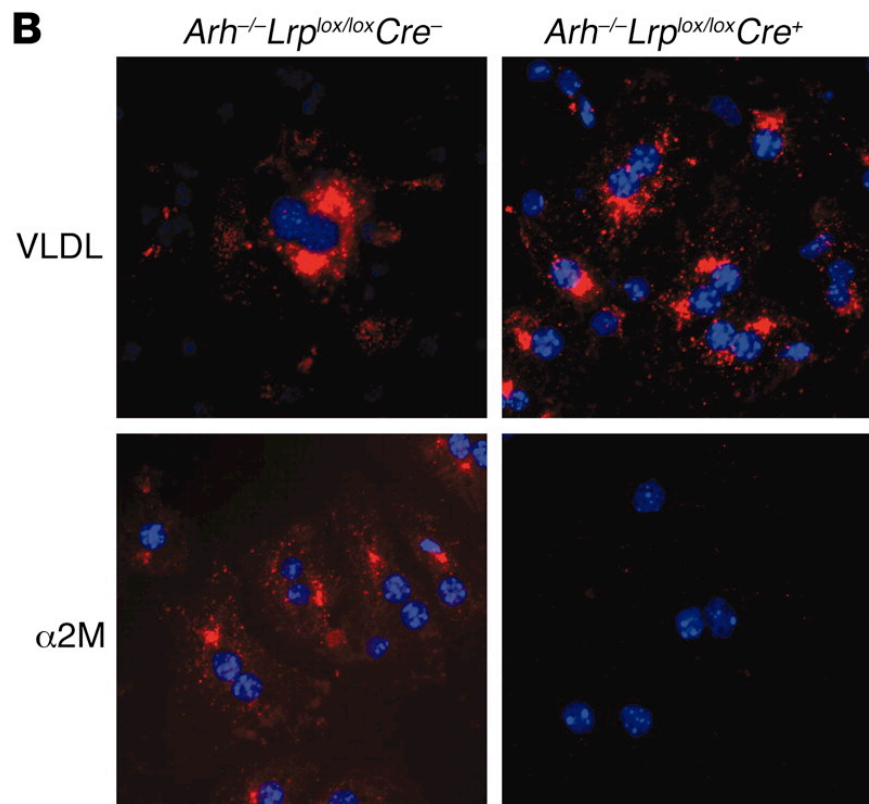
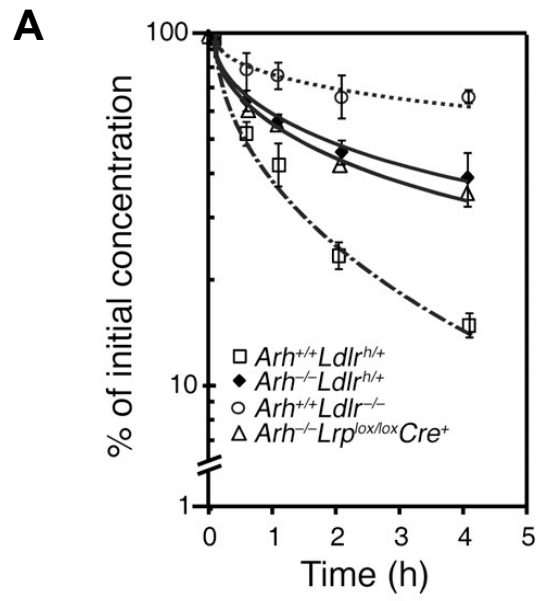


**Figure 6-9:** Deletion of LRP does not reduce  $\beta$ -VLDL clearance in  $Arh^{-/-}$  mice. **(A)** Wild-type ( $\square$ ),  $Arh^{-/-}$  ( $\blacklozenge$ ),  $Ldlr^{-/-}$  ( $\circ$ ), and ( $\triangle$ )  $Arh^{-/-}Lrp^{lox/lox}Cre^{+}$  mice ( $n = 3$  per group) were fasted for 4 hours, anesthetized with sodium pentobarbital, and injected with  $^{125}I$ -labeled rabbit  $\beta$ -VLDL ( $15 \mu\text{g}$ ) via the external jugular vein. Venous blood was collected from the retro-orbital plexus at the indicated times, and the plasma content of isopropanol-precipitable  $^{125}I$ -radioactivity was measured. Radioactivity remaining in the plasma was plotted as a percentage of the activity present 2 minutes after injection of the labeled ligand. The experiment was repeated, and similar results were obtained. **(B)** Primary hepatocytes were isolated from  $Arh^{-/-}Lrp^{lox/lox}Cre^{-}$  and  $Arh^{-/-}Lrp^{lox/lox}Cre^{+}$  mice and incubated overnight in DMEM containing 5% lipoprotein-deficient serum. The next morning, the cells were incubated with  $15 \mu\text{g/ml}$  Dil  $\beta$ -VLDL or  $10 \mu\text{g/ml}$  methylamine-activated  $\alpha 2$ -macroglobulin [82] for 30 minutes. The cells were washed, fixed, and mounted as described in Methods. Images were taken by deconvolution microscopy. Original magnification, x84.

## CHAPTER SEVEN

### Conclusions and Recommendations

To specifically explore the function of ARH in hepatocytes and the intact organism, I have developed an ARH-deficient mouse as an animal model of autosomal recessive hypercholesterolemia. These animals recapitulate central features of the human disease phenotype. When fed normal mouse chow, the *Arh*<sup>-/-</sup> mice are only mildly hypercholesterolemic, but their most striking feature is a profound sensitivity of plasma cholesterol levels to dietary cholesterol intake. On a chow diet the lipoprotein profile from *Arh*<sup>-/-</sup> mice more closely resembles a profile from *Ldlr*<sup>+/-</sup> than *Ldlr*<sup>-/-</sup> mice. In fact, the clinical picture of ARH has been described as intermediate between that of a severe FH heterozygote and an FH homozygote [6]. The plasma levels of LDL are also similar to those of FH homozygotes with an LDLR mutation that is defective for binding of apoB but not apoE [93]. Not until the mice are challenged with a cholesterol-enriched, Western or Paigen-type diets does their LDL cholesterol increase to a level comparable to *Ldlr*<sup>-/-</sup> mice. These data suggest that ARH is of particular importance when LDLR expression is suppressed and is consistent with the considerable benefits ARH patients receive from therapies that increase LDLR expression, such as the statins,

or reduce dietary cholesterol absorption, such as cholestyramine or ezetimibe.

### **Mechanism of hypercholesterolemia in ARH**

ARH patients have LDL FCRs similar to those of FH homozygotes [2]. The clearance of  $^{125}\text{I}$ -LDL from the plasma in *Arh*<sup>-/-</sup> mice is also reduced to a rate comparable that of *Ldlr*<sup>-/-</sup> mice. Two mutations in the cytoplasmic tail of the LDLR, J.D. (Y807C) and FH-Turku (G823D) have been shown to cause FH through distinctly different mechanisms. The J.D. mutation in the NPXY motif of the LDLR disrupts the interaction of ARH with the LDLR tail *in vitro* and leads to the production of a receptor defective in endocytosis in both fibroblasts and hepatocytes [34, 37]. In contrast LDLRs harboring the FH-Turku internalize normally in fibroblasts, but traffic inappropriately to the bile canilicular membrane in hepatocytes, effectively sequestering them from the circulation [83]. From the human studies receptor mislocalization could not be excluded as a cause for the ARH phenotype. In livers from *Arh*<sup>-/-</sup> mice LDLRs appear restricted to the blood sinusoidal surface of the hepatocytes, arguing against a role for ARH in basolateral targeting of the LDLR. The defect in ARH-deficient hepatocytes appears to be one of receptor internalization. Whereas LDLRs are visible not only on the surface but also in vesicular structures

in the cytoplasm of wild-type hepatocytes, the interior of *Arh*<sup>-/-</sup> cells is completely devoid of immunodetectable LDLR. Similarly in immortalized lymphoblasts lacking ARH, a two-fold increase in LDL binding was detected in *Arh*<sup>-/-</sup> lymphoblasts on the cell surface without an increase in total LDLR protein and no LDLR is observed intracellularly [9, 22, 25]. LDLR can be observed in intracellular compartments of *Arh*<sup>-/-</sup> lymphoblasts when ARH is reintroduced via lentiviral infection [9]. These observations are consistent with a model of ARH as an adaptor protein required for LDLR internalization in polarized cells, such as hepatocytes and lymphoblasts. The preserved LDL uptake observed in the fibroblasts of ARH patients but not from the FH patient J.D. suggests that another adaptor not present in the liver may be capable of substituting for ARH in certain cell types.

### **ARH and specificity for the LDLR**

ARH interact with the NPXY sequence of the LDLR. Many of other LDLR family members, such as LRP, megalin, ApoER2, and VLDLR, contain NPXY sequences, yet only the function of the LDLR appears to be impaired *in vivo*. LRP is highly expressed in the liver and aids in the clearance of apoE-containing lipoproteins. The ability to interact with ARH and the similarities in function and endocytosis rate between LRP and

LDLR [74] suggested that LRP function could be mediated by ARH. The clearance of the LRP-specific ligand,  $\alpha$ 2M, however, is normal in ARH-deficient mice, whereas mice lacking hepatic LRP have been shown to have a profound deficiency in  $\alpha$ 2M uptake [80]. In contrast to the striking difference in LDLR distribution between *Arh*<sup>-/-</sup> and wild-type hepatocytes, no alteration in LRP localization was observed. That a receptor functionally and structurally related to the LDLR operates independently of ARH, argues against the ARH phenotype resulting from a global defect in endocytosis. The defect in ARH appears to be restricted to the LDLR. Yet, how receptor specificity is conferred is still unclear. Since the NPXY motifs of other lipoprotein receptor tails are identical in sequence and surrounding residues to the LDLR NPXY, specificity could conceivably be conferred by interaction with other scaffolding proteins that may stabilize the complex through interaction with ARH and the LDLR tail. This hypothesis is consistent with the findings of Praefcke, *et al.* that assembly and internalization of clathrin coated vesicles involves the assembly of adaptors with multiple low-affinity interactions with components of the pit [84]. The low-affinity of individual contacts necessitates the formation of a network of interactions with multiple partners to achieve stability and allows for rapid assembly and disassembly diverse coated pit structures.

### **Role of ARH in clathrin mediated endocytosis**

The results of my complementation assay bear out the rugged energy model Praefcke and colleagues espouse. Mutation of either the pentapeptide clathrin box or the  $\beta_2$ -adapatin binding site fail to ablate LDLR activity, most likely due to redundant binding of clathrin and AP-2 through its  $\beta_2$ -adapatin subunit. Likely the multiple seemingly redundant contacts serve two purposes. First, multiple contacts with clathrin assure that stabilization the interaction between AP-2 and ARH only in the presence of an assembled clathrin lattice, essentially creating a targeting motif for the pair of the clathrin coated pit. Secondly, multiple redundant interactions creates a distribution of residence times for the necessary endocytic machinery components allowing for efficient trapping and high dissociation rates of the constituents [85].

Interestingly, while disruption of the both the clathrin box and the AP-2 binding site led to essentially a null phenotype – the plasma cholesterol levels of the mice remained unchanged over the course of the experiment – disruption of the interaction with the LDLR by mutation the PTB domain appears to have a dominant negative phenotype. Infection with either the F165A and S117Y mutants led to an ~25% increase in plasma cholesterol levels. One possible explanation is that expression of these mutants titrates a binding partner for the LDLR that allows for the

internalization of VLDL. In the absence of ARH or with the L212A/L213A/R266A mutant the hypothetical partner may still bind to the LDLR, and VLDL can be internalized. When the interaction between ARH and the LDLR is disrupted, however, the mutant ARH would compete for this competency factor, reducing the ability of LDLRs to internalize VLDL. An interesting test for this hypothesis would be to follow plasma cholesterol levels after injecting hypercholesterolemic *Arh*<sup>-/-</sup> mice with an adenovirus containing S117Y/L212A/L213A/R266A mutations, effectively eliminating all known partners for ARH. Exacerbation of plasma cholesterol levels would affirm the idea of additional essential partners involved in LDLR endocytosis. Furthermore, this complementation assay could be used to identify the amino acid sequence within ARH necessary for binding and use it to identify the protein, either through biochemical purification of two-hybrid methods.

In addition to AP-2 and clathrin, ARH may play a role in vesicular trafficking during endocytosis. Previously, ARH has been shown to associate with the LDLR during the early stages of endocytosis prior to entry to early endosomes [38]. Consistent with these observations, the majority of ARH co-sediments with rab5 and overlaps EEA1. Rab5 is involved with endocytic internalization and early endosome fusion [86]. Interestingly, the fractions containing the majority of ARH appear apart

from fractions containing the majority of LDLR. Although the peak fractions for ARH and LDLR are distinct, a portion ARH does appear in the LDLR peak fraction. I tested whether the LDLR was required for recruitment of ARH to these specific vesicular structures. ARH associates with plasma membrane vesicles independently of the LDLR, possibly by binding to PtdIns(4,5)P<sub>2</sub> on the inner leaflet of the plasma membrane [38]. ARH may also be recruited to the plasma membrane in the absence of LDLR by association with clathrin and AP-2 [37, 38].

### **Xanthomatosis and cholesterol ester formation**

In order to determine a mechanism for the larger, bulkier xanthomas in ARH, out of proportion to patients' plasma cholesterol levels, I examined VLDL stimulated cholesterol ester synthesis in mouse peritoneal macrophage. Macrophage from *Arh*<sup>-/-</sup> mice accumulate cholesterol esters in response to  $\beta$ -VLDL at a rate indistinguishable to wild type macrophage, whereas cholesterol ester synthesis is greatly retarded in macrophage lacking LDLRs. The increased ability of *Arh*<sup>-/-</sup> macrophage over *Ldlr*<sup>-/-</sup> macrophage to accumulate cholesterol esters in response to VLDL may account for the more severe xanthomatosis observed in ARH patients.

The assay does not predict whether the LDLRs in *Arh*<sup>-/-</sup> macrophage are capable of undergoing clathrin mediated endocytosis. Monocyte-derived macrophage from two siblings with ARH were shown to be defective at LDL internalization [25]; however, VLDL and not LDL is internalized by *Arh*<sup>-/-</sup> hepatocytes. VLDL is normally internalized by LDLR-mediated clathrin coated pit endocytosis [57]. If clathrin mediated endocytosis of LDLRs is defective in *Arh*<sup>-/-</sup> macrophage, LDLRs may decorate the surface of *Arh*<sup>-/-</sup> macrophage, bind VLDL, and be internalized by alternate means. Further characterization is necessary to determine the mechanism of VLDL stimulated cholesterol ester synthesis in *Arh*<sup>-/-</sup> macrophage.

The mice unfortunately did not replicate the more florid formation of xanthomas in ARH compared to FH. Both *Ldlr*<sup>-/-</sup> and *Arh*<sup>-/-</sup> mice developed indistinguishable xanthomatous infiltrates over a similar time course. It may be that the substantial increase in plasma cholesterol levels generated by the Paigen diet overwhelmed any differences that might have been observed between the two genotypes. By feeding the mice a diet less rich in cholesterol one might be able to achieve a range in plasma cholesterol levels where a difference between the two genotypes is apparent. It should be noted, however, that long term maintenance of

the *Arh*<sup>-/-</sup> and *Ldlr*<sup>-/-</sup> mice on the Western diet failed to stimulate xanthoma formation in either genotype (data not shown).

### **VLDL metabolism in ARH**

It is of interest that the plasma cholesterol levels in the *Arh*<sup>-/-</sup> mice are only mildly elevated on a chow diet despite the mice having a rate of clearance of LDL as low as mice with no functional LDLRs. Although the fractional catabolic rate of LDL is equivalent to that of *Ldlr*<sup>-/-</sup> mice, VLDL clearance is partially preserved. The effective clearance of VLDL appears to partially protect the *Arh*<sup>-/-</sup> animals from hypercholesterolemia when fed a carbohydrate-enriched diet to stimulate triglyceride production, whereas *Ldlr*<sup>-/-</sup> mice accumulate a profound amount of cholesterol-rich  $\beta$ -VLDL. Similarly, mice overexpressing sterol regulatory element binding protein-1a (SREBP-1a), in which triglyceride synthetic genes are constitutively up-regulated, are protected from hyperlipidemia as long as LDLR function is preserved [47]. When SREBP-1a transgenic mice were bred onto an *Ldlr*<sup>-/-</sup> background, the animals accumulated cholesterol-dense  $\beta$ -VLDL similar to our *Ldlr*<sup>-/-</sup> mice fed the high-carbohydrate diet. Interestingly, the *Arh*<sup>-/-</sup> mice do show and accumulation of LDL not present in the wild-type animals, consistent with a delay in removal from the circulation once VLDL is converted to LDL.

While *Arh*<sup>-/-</sup> mice have significantly lower LDL-C levels than *Ldlr*<sup>-/-</sup> mice when fed normal chow, the lipid profiles of the two genotypes become indistinguishable once challenged with cholesterol feeding. Under conditions of cholesterol feeding, *Ldlr* expression is suppressed, increasing the residence time of VLDL in the circulation and leading to greater conversion of VLDL remnants to LDL. This model implies increasing *Ldlr* expression, even in the absence of ARH, should result in lower levels of LDL-C by the removal of the precursors to LDL formation. The increased clearance of VLDL and VLDL remnants due to increased *LDLR* expression may explain the more potent response to HMG-CoA reductase inhibitors (statins) of ARH than homozygous FH patients [6, 11, 17, 18].

Electron microscopy of colloidal gold-labeled lipoproteins revealed the clearance of VLDL in the *Arh*<sup>-/-</sup> mice is primarily mediated by the liver and not extrahepatic tissues. The preferential internalization of VLDL over LDL is replicated *in vitro* by primary hepatocytes isolated from *Arh*<sup>-/-</sup> animals. This result does not agree with a report from another group that *Arh*<sup>-/-</sup> hepatocytes grown *in vitro* are competent at LDL internalization [87]. Possible explanations for this difference are alterations in hepatocyte gene expression due to the longer time (>48 h v. 16 h) of the hepatocytes in culture before addition of lipoprotein in their assay and the possible

presence in their assay of LDL aggregates, which I found were internalized similarly to VLDL and removed via FPLC prior to addition to the cells (data not shown).

VLDL particles contain multiple apoE moieties and binds with higher affinity to the LDLR than the single recognition site of apoB [88]. Previously, Michaely, *et al.* reported reduced capacity for LDL relative to VLDL and IgG-C7 on the surface of *ARH*<sup>-/-</sup> lymphocytes, suggesting ARH may act as a competency factor for LDL binding. *Arh*<sup>-/-</sup> *Ldlr*<sup>h/h</sup> hepatocytes bound but did not internalize IgG-C7, suggesting the high-affinity binding of VLDL is not sufficient for internalization. VLDL internalization in ARH may be mediated by the multiple apoE peptides on VLDL clustering LDLRs. Clustering of ApoER2 or VLDLR, two closely related LDLR family members, has been shown to be sufficient for signaling through the PTB domain-containing adaptor protein, Dab1 [89]. Using Protein A, I assembled tetramers of the monoclonal anti-LDLR antibody, IgG-C7, as a multivalent surrogate ligand for VLDL. IgG-C7 tetramers bound efficiently to the surface of *Arh*<sup>-/-</sup> *Ldlr*<sup>h/h</sup> hepatocytes, but the complexes failed to be internalized at 37°C. The lack of internalized IgG-C7:Protein A tetramers argues strongly against, but does not rule out, LDLR clustering as the mode of VLDL internalization. The multiple apoE

moieties on VLDL may adopt a conformation required for LDLR endocytosis that our antibody complexes were unable to replicate.

Alternatively, VLDL may bind the LDLRs which decorate the surface of *Arh*<sup>-/-</sup> hepatocytes until a co-receptor binds to additional apoE moieties on the VLDL particle and internalizes the complex. While LRP is an attractive candidate for a co-receptor, *Arh*<sup>-/-</sup> mice with a liver specific deletion of LRP did not demonstrate a decrease rate of VLDL clearance compared to mice expressing LRP. A second candidate coreceptor are heparin sulfate proteoglycans (HSPGs). Typically lipoprotein remnants must be highly enriched in apoE to bind to HSPGs with high affinity. Enrichment with apoE3 enhanced binding of  $\beta$ -VLDL to HepG2 cells 12-fold over  $\beta$ -VLDL without added apoE or LDL [90]. This enhancement in binding is heparinase sensitive, and the remaining high affinity binding is due to the LDLR.

In ARH the 15-20 fold more LDLR present at the cell surface in ARH [91], may eliminate the need for apoE enrichment of lipoprotein remnants before sequestration at the cell surface. VLDL particles may bind the LDLRs decorating the cell surface and remain bound with high affinity until they become sufficiently enriched with apoE to be internalized by HSPG or hepatic lipase mediated pathways. Intravenous heparinase treatment retards  $\beta$ -VLDL clearance ~2 fold in wild type mice [92]. A

similar experiment in the *Arh*<sup>-/-</sup> mice would be of interest to determine whether HSPGs are responsible for the preservation of  $\beta$ -VLDL clearance on an *Arh*<sup>-/-</sup> background.

## **Conclusions**

While the genetic and metabolic studies in humans have been revealing, detailed cell biological studies have been restricted to peripheral tissues, such as fibroblasts and lymphoblasts. The defect in hepatocytes, which is responsible for the ARH phenotype, can now be examined in molecular detail using the *Arh*<sup>-/-</sup> mouse model. Immunolocalization confirmed normal trafficking of the LDLR but defective endocytosis as the etiology of the cholesterol elevations in ARH. Whole animal studies using the *Arh*<sup>-/-</sup> mice have revealed that differential handling of VLDL and LDL as the basis for the lower plasma cholesterol levels observed in ARH patients than FH homozygotes. In addition, the LDLR-dependent removal of VLDL explains both the dietary sensitivity of the mice and the effectiveness with which lipid lower drugs, such as ezetimibe and the statins, work in ARH patients.



## BIBLIOGRAPHY

1. Khachadurian, A.K., and Uthman, S.M. (1973). Experiences with the homozygous cases of familial hypercholesterolemia. A report of 52 patients. *Nutr Metab* **15**, 132-140.
2. Zuliani, G., Arca, M., Signore, A., Bader, G., Fazio, S., Chianelli, M., Bellosta, S., Campagna, F., Montali, A., Maioli, M., Pacifico, A., Ricci, G., and Fellin, R. (1999). Characterization of a new form of inherited hypercholesterolemia: familial recessive hypercholesterolemia. *Arterioscler Thromb Vasc Biol* **19**, 802-809.
3. Zuliani, G., Vigna, G.B., Corsini, A., Maioli, M., Romagnoni, F., and Fellin, R. (1995). Severe hypercholesterolaemia: unusual inheritance in an Italian pedigree. *Eur J Clin Invest* **25**, 322-331.
4. Goldstein, J., Hobbs, H., and Brown, M. (2001). Familial hypercholesterolemia. In *The Metabolic and Molecular Bases of Inherited Disease, Volume II, 8th Edition*, C. Scriver, A. Beaudet, W. Sly and D. Valle, eds. (New York: McGraw Hill), pp. 2683-2913.
5. Gagne, C., Gaudet, D., Bruckert, E., and for the Ezetimibe Study Group (2002). Efficacy and Safety of Ezetimibe Coadministered With Atorvastatin or Simvastatin in Patients With Homozygous Familial Hypercholesterolemia. *Circulation* **105**, 2469-2475.

6. Arca, M., Zuliani, G., Wilund, K., Campagna, F., Fellin, R., Bertolini, S., Calandra, S., Ricci, G., Glorioso, N., Maioli, M., Pintus, P., Carru, C., Cossu, F., Cohen, J., and Hobbs, H.H. (2002). Autosomal recessive hypercholesterolaemia in Sardinia, Italy, and mutations in ARH: a clinical and molecular genetic analysis. *Lancet* **359**, 841-847.
7. Harada-Shiba, M., Takagi, A., Miyamoto, Y., Tsushima, M., Ikeda, Y., Yokoyama, S., and Yamamoto, A. (2003). Clinical Features and Genetic Analysis of Autosomal Recessive Hypercholesterolemia. *J Clin Endocrinol Metab* **88**, 2541-2547.
8. Harada-Shiba, M., Tajima, S., Yokoyama, S., Miyake, Y., Kojima, S., Tsushima, M., Kawakami, M., and Yamamoto, A. (1992). Siblings with normal LDL receptor activity and severe hypercholesterolemia. *Arterioscler Thromb* **12**, 1071-1078.
9. Eden, E.R., Patel, D.D., Sun, X.M., Burden, J.J., Themis, M., Edwards, M., Lee, P., Neuwirth, C., Naoumova, R.P., and Soutar, A.K. (2002). Restoration of LDL receptor function in cells from patients with autosomal recessive hypercholesterolemia by retroviral expression of ARH1. *J Clin Invest* **110**, 1695-1702.
10. Garcia, C.K., Wilund, K., Arca, M., Zuliani, G., Fellin, R., Maioli, M., Calandra, S., Bertolini, S., Cossu, F., Grishin, N., Barnes, R.,

- Cohen, J.C., and Hobbs, H.H. (2001). Autosomal recessive hypercholesterolemia caused by mutations in a putative LDL receptor adaptor protein. *Science* **292**, 1394-1398.
11. Naoumova, R.P., Neuwirth, C., Lee, P., Miller, J.P., Taylor, K.G., and Soutar, A.K. (2004). Autosomal recessive hypercholesterolaemia: long-term follow up and response to treatment. *Atherosclerosis* **174**, 165-172.
12. Schmidt, H.H., Stuhmann, M., Shamburek, R., Schewe, C.K., Ebhardt, M., Zech, L.A., Buttner, C., Wendt, M., Beisiegel, U., Brewer, H.B., Jr., and Manns, M.P. (1998). Delayed low density lipoprotein (LDL) catabolism despite a functional intact LDL-apolipoprotein B particle and LDL-receptor in a subject with clinical homozygous familial hypercholesterolemia. *J Clin Endocrinol Metab* **83**, 2167-2174.
13. Lind, S., Olsson, A.G., Eriksson, M., Rudling, M., Eggertsen, G., and Angelin, B. (2004). Autosomal recessive hypercholesterolaemia: normalization of plasma LDL cholesterol by ezetimibe in combination with statin treatment. *J Intern Med* **256**, 406-412.
14. Soutar, A.K., Naoumova, R.P., and Traub, L.M. (2003). Genetics, Clinical Phenotype, and Molecular Cell Biology of Autosomal

- Recessive Hypercholesterolemia. *Arterioscler Thromb Vasc Biol* **23**, 1963-1970.
15. Uauy, R., Vega, G.L., Grundy, S.M., and Bilheimer, D.M. (1988). Lovastatin therapy in receptor-negative homozygous familial hypercholesterolemia: lack of effect on low-density lipoprotein concentrations or turnover. *J Pediatr* **113**, 387-392.
  16. Yamamoto, A., Yamamura, T., Yokoyama, S., Sudo, H., and Matsuzawa, Y. (1984). Combined drug therapy--cholestyramine and compactin--for familial hypercholesterolemia. *Int J Clin Pharmacol Ther Toxicol* **22**, 493-497.
  17. Raal, F.J., Pappu, A.S., Illingworth, D.R., Pilcher, G.J., Marais, A.D., Firth, J.C., Kotze, M.J., Heinonen, T.M., and Black, D.M. (2000). Inhibition of cholesterol synthesis by atorvastatin in homozygous familial hypercholesterolaemia. *Atherosclerosis* **150**, 421.
  18. Raal, F.J., Pilcher, G.J., Illingworth, D.R., Pappu, A.S., Stein, E.A., Laskarzewski, P., Mitchel, Y.B., and Melino, M.R. (1997). Expanded-dose simvastatin is effective in homozygous familial hypercholesterolaemia. *Atherosclerosis* **135**, 249.
  19. Al-Kateb, H., Bahring, S., Hoffmann, K., Strauch, K., Busjahn, A., Nurnberg, G., Jouma, M., Bautz, E.K.F., Dresel, H.A., and Luft,

- F.C. (2002). Mutation in the ARH Gene and a Chromosome 13q Locus Influence Cholesterol Levels in a New Form of Digenic-Recessive Familial Hypercholesterolemia. *Circ Res* **90**, 951-958.
20. Al-Kateb, H., Bautz, E.K.F., Luft, F.C., and Bähring, S. (2003). A Splice Mutation in a Syrian Autosomal Recessive Hypercholesterolemia Family Causes a Two-Nucleotide Deletion of mRNA. *Circ Res* **93**, 49e-50.
21. Tietge, U.J.F., Genschel, J., and Schmidt, H.H.J. (2003). A Q136Stop mutation in the ARH gene causing autosomal recessive hypercholesterolaemia with severely delayed LDL catabolism. *Journal of Internal Medicine* **253**, 582-583.
22. Wilund, K.R., Yi, M., Campagna, F., Arca, M., Zuliani, G., Fellin, R., Ho, Y.K., Garcia, J.V., Hobbs, H.H., and Cohen, J.C. (2002). Molecular mechanisms of autosomal recessive hypercholesterolemia. *Hum Mol Genet* **11**, 3019-3030.
23. Goldstein, J.L., Brown, M.S., Anderson, R.G.W., Russell, D.W., and Schneider, W.J. (1985). Receptor-Mediated Endocytosis: Concepts Emerging from the LDL Receptor System. *Annual Review of Cell Biology* **1**, 1-39.
24. Soutar, A.K., and Knight, B.L. (1982). Degradation by cultured monocyte-derived macrophages from normal and familial

- hypercholesterolaemic subjects of modified and unmodified low-density lipoproteins. *Biochem J* **204**, 549-556.
25. Norman, D., Sun, X.-M., Bourbon, M., Knight, B.L., Naoumova, R.P., and Soutar, A.K. (1999). Characterization of a novel cellular defect in patients with phenotypic homozygous familial hypercholesterolemia. *J Clin Invest* **104**, 619-628.
  26. Dell'Angelica, E.C. (2001). Clathrin-binding proteins: Got a motif? Join the network! *Trends in Cell Biology* **11**, 315.
  27. Chen, W.J., Goldstein, J.L., and Brown, M.S. (1990). NPXY, a sequence often found in cytoplasmic tails, is required for coated pit-mediated internalization of the low density lipoprotein receptor. *J Biol Chem* **265**, 3116-3123.
  28. Forman-Kay, J.D., and Pawson, T. (1999). Diversity in protein recognition by PTB domains. *Curr Opin Struct Biol* **9**, 690-695.
  29. Mishra, S.K., Keyel, P.A., Hawryluk, M.J., Agostinelli, N.R., Watkins, S.C., and Traub, L.M. (2002). Disabled-2 exhibits the properties of a cargo-selective endocytic clathrin adaptor. *EMBO J* **21**, 4915-4926.
  30. Morris, S.M., Tallquist, M.D., Rock, C.O., and Cooper, J.A. (2002). Dual roles for the Dab2 adaptor protein in embryonic development and kidney transport. *EMBO J* **21**, 1555-1564.

31. Nagai, M., Meerloo, T., Takeda, T., and Farquhar, M.G. (2003). The Adaptor Protein ARH Escorts Megalin to and through Endosomes. *Mol. Biol. Cell*, **14**, 4984-96.
32. Herz, J., and Bock, H.H. (2002). Lipoprotein receptors in the nervous system. *Annu Rev Biochem* **71**, 405-434.
33. Leheste, J.R., Melsen, F., Wellner, M., Jansen, P., Schlichting, U., Renner-Muller, I., Andreassen, T.T., Wolf, E., Bachmann, S., Nykjaer, A., and Willnow, T.E. (2003). Hypocalcemia and osteopathy in mice with kidney-specific megalin gene defect. *FASEB J*, **17**, 247-9.
34. Davis, C.G., Lehrman, M.A., Russell, D.W., Anderson, R.G., Brown, M.S., and Goldstein, J.L. (1986). The J.D. mutation in familial hypercholesterolemia: amino acid substitution in cytoplasmic domain impedes internalization of LDL receptors. *Cell* **45**, 15-24.
35. Garcia-Garcia, A.B., Real, J.T., Puig, O., Cebolla, E., Marin-Garcia, P., Martinez Ferrandis, J.I., Garcia-Sogo, M., Civera, M., Ascaso, J.F., Carmena, R., Armengod, M.E., and Chaves, F.J. (2001). Molecular genetics of familial hypercholesterolemia in Spain: Ten novel LDLR mutations and population analysis. *Hum Mutat* **18**, 458-459.

36. Brown, M.S., and Goldstein, J.L. (1976). Analysis of a mutant strain of human fibroblasts with a defect in the internalization of receptor-bound low density lipoprotein. *Cell* **9**, 663-674.
37. He, G., Gupta, S., Yi, M., Michaely, P., Hobbs, H.H., and Cohen, J.C. (2002). ARH is a modular adaptor protein that interacts with the LDL receptor, clathrin, and AP-2. *J Biol Chem* **277**, 44044-44049.
38. Mishra, S.K., Watkins, S.C., and Traub, L.M. (2002). The autosomal recessive hypercholesterolemia (ARH) protein interfaces directly with the clathrin-coat machinery. *Proc Natl Acad Sci U S A* **99**, 16099-16104.
39. Rohlmann, A., Gotthardt, M., Hammer, R.E., and Herz, J. (1998). Inducible Inactivation of Hepatic LRP Gene by Cre-mediated Recombination Confirms Role of LRP in Clearance of Chylomicron Remnants. *J Clin Invest* **101**, 689-695.
40. ter Haar, E., Harrison, S.C., and Kirchhausen, T. (2000). From the Cover: Peptide-in-groove interactions link target proteins to the beta-propeller of clathrin. *Proc Natl Acad Sci U S A* **97**, 1096-1100.
41. Gaidarov, I., Krupnick, J.G., Falck, J.R., Benovic, J.L., and Keen, J.H. (1999). Arrestin function in G protein-coupled receptor

- endocytosis requires phosphoinositide binding. *EMBO J* **18**, 871-881.
42. Kim, Y.-M., and Benovic, J.L. (2002). Differential Roles of Arrestin-2 Interaction with Clathrin and Adaptor Protein 2 in G Protein-coupled Receptor Trafficking. *J Biol Chem* **277**, 30760-30768.
  43. Laporte, S.A., Miller, W.E., Kim, K.-M., and Caron, M.G. (2002). beta -Arrestin/AP-2 Interaction in G Protein-coupled Receptor Internalization. IDENTIFICATION OF A beta -ARRESTIN BINDING SITE IN beta 2-ADAPTIN. *J Biol Chem* **277**, 9247-9254.
  44. Sambrook, J., and Russel, D.W. (2001). *Molecular Cloning: A Laboratory Manual* (Cold Spring Harbor, New York: Cold Spring Harbor Laboratory Press).
  45. Shimano, H., Horton, J.D., Hammer, R.E., Shimomura, I., Brown, M.S., and Goldstein, J.L. (1996). Overproduction of Cholesterol and Fatty Acids Causes Massive Liver Enlargement in Transgenic Mice Expressing Truncated SREBP-1a. *J Clin Invest* **98**, 1575-1584.
  46. Yokode, M., Hammer, R.E., Ishibashi, S., Brown, M.S., and Goldstein, J.L. (1990). Diet-induced hypercholesterolemia in mice: prevention by overexpression of LDL receptors. *Science* **250**, 1273-1275.

47. Horton, J.D., Shimano, H., Hamilton, R.L., Brown, M.S., and Goldstein, J.L. (1999). Disruption of LDL receptor gene in transgenic SREBP-1a mice unmasks hyperlipidemia resulting from production of lipid-rich VLDL. *J Clin Invest* **103**, 1067-1076.
48. Butcher, E.C., and Lowry, O.H. (1976). Measurement of nanogram quantities of protein by hydrolysis followed by reaction with orthophthalaldehyde or determination of glutamate. *Anal Biochem* **76**, 502-523.
49. Fraker, P.J., and Speck, J.C., Jr. (1978). Protein and cell membrane iodinations with a sparingly soluble chloroamide, 1,3,4,6-tetrachloro-3a,6a-diphrenylglycoluril. *Biochem Biophys Res Commun* **80**, 849-857.
50. Herz, J., Hamann, U., Rogne, S., Myklebost, O., Gausepohl, H., and Stanley, K.K. (1988). Surface location and high affinity for calcium of a 500-kd liver membrane protein closely related to the LDL-receptor suggest a physiological role as lipoprotein receptor. *EMBO J* **7**, 4119-4127.
51. Russell, D.W., Schneider, W.J., Yamamoto, T., Luskey, K.L., Brown, M.S., and Goldstein, J.L. (1984). Domain map of the LDL receptor: sequence homology with the epidermal growth factor precursor. *Cell* **37**, 577-585.

52. Beisiegel, U., Schneider, W., Goldstein, J., Anderson, R., and Brown, M. (1981). Monoclonal antibodies to the low density lipoprotein receptor as probes for study of receptor-mediated endocytosis and the genetics of familial hypercholesterolemia. *J Biol Chem* **256**, 11923-11931.
53. Beisiegel, U., Schneider, W., Brown, M., and Goldstein, J. (1982). Immunoblot analysis of low density lipoprotein receptors in fibroblasts from subjects with familial hypercholesterolemia. *J Biol Chem* **257**, 13150-13156.
54. Ishibashi, S., Brown, M.S., Goldstein, J.L., Gerard, R.D., Hammer, R.E., and Herz, J. (1993). Hypercholesterolemia in low density lipoprotein receptor knockout mice and its reversal by adenovirus-mediated gene delivery. *J Clin Invest* **92**, 883-893.
55. Knouff, C., Malloy, S., Wilder, J., Altenburg, M.K., and Maeda, N. (2001). Doubling Expression of the Low Density Lipoprotein Receptor by Truncation of the 3'-Untranslated Region Sequence Ameliorates Type III Hyperlipoproteinemia in Mice Expressing the Human ApoE2 Isoform. *J Biol Chem* **276**, 3856-3862.
56. Goldstein, J.L., Basu, S.K., and Brown, M.S. (1983). Receptor-mediated endocytosis of low-density lipoprotein in cultured cells. *Methods Enzymol* **98**, 241-260.

57. Perrey, S., Ishibashi, S., Kitamine, T., Osuga, J.-i., Yagyu, H., Chen, Z., Shionoiri, F., Iizuka, Y., Yahagi, N., and Tamura, Y. (2001). The LDL receptor is the major pathway for [beta]-VLDL uptake by mouse peritoneal macrophages. *Atherosclerosis* **154**, 51-60.
58. Kovanen, P.T., Brown, M.S., Basu, S.K., Bilheimer, D.W., and Goldstein, J.L. (1981). Saturation and suppression of hepatic lipoprotein receptors: a mechanism for the hypercholesterolemia of cholesterol-fed rabbits. *Proc Natl Acad Sci U S A* **78**, 1396-1400.
59. Bolton, A.E., and Hunter, W.M. (1973). The labelling of proteins to high specific radioactivities by conjugation to a <sup>125</sup>I-containing acylating agent. *Biochem J* **133**, 529-539.
60. Krieger, M., Smith, L.C., Anderson, R.G., Goldstein, J.L., Kao, Y.J., Pownall, H.J., Gotto, A.M., Jr., and Brown, M.S. (1979). Reconstituted low density lipoprotein: a vehicle for the delivery of hydrophobic fluorescent probes to cells. *J Supramol Struct* **10**, 467-478.
61. Pitas, R.E., Innerarity, T.L., Weinstein, J.N., and Mahley, R.W. (1981). Acetoacetylated lipoproteins used to distinguish fibroblasts from macrophages in vitro by fluorescence microscopy. *Arteriosclerosis* **1**, 177-185.

62. Pathak, R.K., Yokode, M., Hammer, R.E., Hofmann, S.L., Brown, M.S., Goldstein, J.L., and Anderson, R.G. (1990). Tissue-specific sorting of the human LDL receptor in polarized epithelia of transgenic mice. *J Cell Biol* **111**, 347-359.
63. Gotthardt, M., Hammer, R.E., Hubner, N., Monti, J., Witt, C.C., McNabb, M., Richardson, J.A., Granzier, H., Labeit, S., and Herz, J. (2003). Conditional Expression of Mutant M-line Titins Results in Cardiomyopathy with Altered Sarcomere Structure. *J Biol Chem* **278**, 6059-6065.
64. Soriano, P., Montgomery, C., Geske, R., and Bradley, A. (1991). Targeted disruption of the c-src proto-oncogene leads to osteopetrosis in mice. *Cell* **64**, 693-702.
65. Mansour, S.L., Thomas, K.R., and Capecchi, M.R. (1988). Disruption of the proto-oncogene int-2 in mouse embryo-derived stem cells: a general strategy for targeting mutations to non-selectable genes. *Nature* **336**, 348-352.
66. Willnow, T.E., and Herz, J. (1994). Homologous recombination for gene replacement in mouse cell lines. *Methods Cell Biol* **43 Pt A**, 305-334.
67. Choi, S.Y., and Cooper, A.D. (1993). A comparison of the roles of the low density lipoprotein (LDL) receptor and the LDL receptor-

- related protein/alpha 2-macroglobulin receptor in chylomicron remnant removal in the mouse in vivo. *J Biol Chem* **268**, 15804-15811.
68. Bannerman, R.M. (1983). Hematology. In *The Mouse in Biomedical Research*, Volume III, H.L. Foster, J.D. Small and J.G. Fox, eds. (New York: Academic Press), pp. 294-312.
69. Gotthardt, M., Trommsdorff, M., Nevitt, M.F., Shelton, J., Richardson, J.A., Stockinger, W., Nimpf, J., and Herz, J. (2000). Interactions of the Low Density Lipoprotein Receptor Gene Family with Cytosolic Adaptor and Scaffold Proteins Suggest Diverse Biological Functions in Cellular Communication and Signal Transduction. *J Biol Chem* **275**, 25616-25624.
70. Stockinger, W., Sailer, B., Strasser, V., Recheis, B., Fasching, D., Kahr, L., Schneider, W.J., and Nimpf, J. (2002). The PX-domain protein SNX17 interacts with members of the LDL receptor family and modulates endocytosis of the LDL receptor. *EMBO J* **21**, 4259-4267.
71. Basu, S.K., Goldstein, J.L., Anderson, R.G.W., and Brown, M.S. (1976). Degradation of Cationized Low Density Lipoprotein and Regulation of Cholesterol Metabolism in Homozygous Familial

- Hypercholesterolemia Fibroblasts. *Proc Natl Acad Sci U S A* **73**, 3178-3182.
72. Herz, J., and Gerard, R. (1993). Adenovirus-Mediated Transfer of Low Density Lipoprotein Receptor Gene Acutely Accelerates Cholesterol Clearance in Normal Mice. *Proc Natl Acad Sci U S A* **90**, 2812-2816.
73. Schagger, H., and von Jagow, G. (1991). Blue native electrophoresis for isolation of membrane protein complexes in enzymatically active form. *Anal Biochem* **199**, 223-231.
74. Li, Y., Lu, W., Marzolo, M.P., and Bu, G. (2001). Differential Functions of Members of the Low Density Lipoprotein Receptor Family Suggested by Their Distinct Endocytosis Rates. *J Biol Chem* **276**, 18000-18006.
75. Kishimoto, A., Brown, M., Slaughter, C., and Goldstein, J. (1987). Phosphorylation of serine 833 in cytoplasmic domain of low density lipoprotein receptor by a high molecular weight enzyme resembling casein kinase II. *J Biol Chem* **262**, 1344-1351.
76. Yokode, M., Pathak, R.K., Hammer, R.E., Brown, M.S., Goldstein, J.L., and Anderson, R.G. (1992). Cytoplasmic sequence required for basolateral targeting of LDL receptor in livers of transgenic mice. *J Cell Biol* **117**, 39-46.

77. Stolt, P.C., Jeon, H., Song, H.K., Herz, J., Eck, M.J., and Blacklow, S.C. (2003). Origins of Peptide Selectivity and Phosphoinositide Binding Revealed by Structures of Disabled-1 PTB Domain Complexes. *Structure* **11**, 569-579.
78. Stolt, P.C., Vardar, D., and Blacklow, S.C. (2004). The dual-function disabled-1 PTB domain exhibits site independence in binding phosphoinositide and peptide ligands. *Biochemistry* **43**, 10979-10987.
79. Twisk, J., Gillian-Daniel, D.L., Tebon, A., Wang, L., Barrett, P.H.R., and Attie, A.D. (2000). The role of the LDL receptor in apolipoprotein B secretion. *J Clin Invest* **105**, 521-532.
80. Rohlmann, A., Gotthardt, M., Willnow, T.E., Hammer, R.E., and Herz, J. (1996). Sustained somatic gene inactivation by viral transfer of Cre recombinase. *Nat Biotechnol* **14**, 1562-1565.
81. Yakar, S., Liu, J.-L., Stannard, B., Butler, A., Accili, D., Sauer, B., and LeRoith, D. (1999). Normal growth and development in the absence of hepatic insulin-like growth factor I. *Proc Natl Acad Sci U S A* **96**, 7324-7329.
82. Imber, M.J., and Pizzo, S.V. (1981). Clearance and binding of two electrophoretic "fast" forms of human alpha 2-macroglobulin. *J Biol Chem* **256**, 8134-8139.

83. Koivisto, U.M., Hubbard, A.L., and Mellman, I. (2001). A novel cellular phenotype for familial hypercholesterolemia due to a defect in polarized targeting of LDL receptor. *Cell* **105**, 575-585.
84. Praefcke, G.J., Ford, M.G., Schmid, E.M., Olesen, L.E., Gallop, J.L., Peak-Chew, S.Y., Vallis, Y., Babu, M.M., Mills, I.G., and McMahon, H.T. (2004). Evolving nature of the AP2 alpha-appendage hub during clathrin-coated vesicle endocytosis. *EMBO J* **23**, 4371-4383.
85. Licht, S.S., Sonnleitner, A., Weiss, S., and Schultz, P.G. (2003). A Rugged Energy Landscape Mechanism for Trapping of Transmembrane Receptors during Endocytosis. *Biochemistry* **42**, 2916-2925.
86. Somsel Rodman, J., and Wandinger-Ness, A. (2000). Rab GTPases coordinate endocytosis. *J Cell Sci* **113**, 183-192.
87. Harada-Shiba, M., Takagi, A., Marutsuka, K., Moriguchi, S., Yagyu, H., Ishibashi, S., Asada, Y., and Yokoyama, S. (2004). Disruption of Autosomal Recessive Hypercholesterolemia Gene Shows Different Phenotype In Vitro and In Vivo. *Circ Res* **95**, 945-952.
88. Mahley, R.W. (1988). Apolipoprotein E: cholesterol transport protein with expanding role in cell biology. *Science* **240**, 622-630.

89. Strasser, V., Fasching, D., Hauser, C., Mayer, H., Bock, H.H., Hiesberger, T., Herz, J., Weeber, E.J., Sweatt, J.D., Pramatarova, A., Howell, B., Schneider, W.J., and Nimpf, J. (2004). Receptor Clustering Is Involved in Reelin Signaling. *Mol Cell Biol* **24**, 1378-1386.
90. Mahley, R.W., and Ji, Z.-S. (1999). Remnant lipoprotein metabolism: key pathways involving cell-surface heparan sulfate proteoglycans and apolipoprotein E. *J Lipid Res* **40**, 1-16.
91. Michaely, P., Li, W.-P., Anderson, R.G.W., Cohen, J.C., and Hobbs, H.H. (2004). The Modular Adaptor Protein ARH Is Required for Low Density Lipoprotein (LDL) Binding and Internalization but Not for LDL Receptor Clustering in Coated Pits. *J Biol Chem* **279**, 34023-34031.
92. Ji, Z.S., Sanan, D.A., and Mahley, R.W. (1995). Intravenous heparinase inhibits remnant lipoprotein clearance from the plasma and uptake by the liver: in vivo role of heparan sulfate proteoglycans. *J Lipid Res* **36**, 583-592.
93. Levy E, Minnich A, Cacan SL, Thibault L, Giroux LM, Davignon J, Lambert M. Association of an exon 3 mutation (Trp66-->Gly) of the LDL receptor with variable expression of familial

hypercholesterolemia in a French Canadian family. (1997) *Biochem Mol Med* **60**, 59-69.

